TECHNISCHE
UNIVERSITÄT
WIEN
Vienna University of Technology

DIPLOMARBEIT

The Floquet Wigner-Smith Operator for Time-Periodic Systems

zur Erlangung des akademischen Grades

Diplom-Ingenieur

im Rahmen des Studiums

066 461 Masterstudium Technische Physik

ausgeführt am Institut für Theoretische Physik
der Technischen Universität Wien

unter der Anleitung von
Univ.Prof. Dipl.-Ing. Dr.techn. Stefan Rotter
Univ.Ass. Dipl.-Ing. Matthias Kühmayer, BSc
Univ.Ass. Dipl.-Ing. Matthias Zens, BSc

durch

David Globosits, BSc
e01525314

Hetzendorfer Straße 93/6/3
1120 Wien

12.09.2021

Unterschrift Verfasser

Unterschrift Betreuer

Abstract

The manipulation of small objects with waves is of great interest in various fields of science including, e.g., medicine and biology. Recently a theory based on the generalized Wigner-Smith (GWS) operator was developed, where the knowledge of the scattering matrix of a static system is enough to find optimal states for micromanipulation. In the present thesis, we extend this concept to time-periodic Floquet-setups. For such systems a unitary scattering matrix can be found, too, which we use to introduce the Floquet Wigner-Smith (FWS) operator. To illustrate the operative principle of our theory, we apply this new operator to four different potentials. We start with the simple case of a Dirac delta potential oscillating in strength or position. Due to the pointlike interaction region, such potentials are convenient to handle. We then look at more realistic setups of an extended rectangular barrier. We study a rectangular potential barrier also oscillating in strength or position. The eigenstates of the FWS operators in all of the above cases develop properties, which are favourable for the micromanipulation of periodically moving objects. We can interpret the specific behaviour of those eigenstates since they share a strong connection to their static GWS counterparts.

Kurzzusammenfassung

In vielen naturwissenschaftlichen Gebieten, wie zum Beispiel Medizin oder Biologie, gibt es starkes Interesse daran, kleine Objekte mit Hilfe von Wellen zu manipulieren. Basierend auf dem sogenannten generalisierten Wigner-Smith (GWS) Operator konnte vor Kurzem eine Theorie entwickelt werden, bei der das Wissen um die Streumatrix eines statischen Systems genügt, um optimale Zustände für die Mikromanipulation zu finden. In dieser Diplomarbeit verallgemeinern wir diese Konzepte auf periodisch zeitabhängige Systeme, sogenannte Floquet-Systeme. Da auch in diesen Systemen eine unitäre Streumatrix zu finden ist, ist die Verallgemeinerung auf eine konsistente Art und Weise möglich. Wir nutzen diese Streumatrix, um den Floquet Wigner-Smith (FWS) Operator einzuführen. Wir wenden unsere Theorie auf vier verschiedenen Potentialen an, um das operative Prinzip vorzustellen. Dafür untersuchen wir den Fall eines Dirac-Delta Potentials, das im Ort oder in der Stärke oszilliert. Wir wählen zunächst diese Potentiale, da ihre Streuregionen jeweils nur ein Punkt sind, was eine einfache Beschreibung zulässt. Nachdem wir diese verstanden haben, betrachten wir realistischere Systeme, die eine ausgedehnte Streuregion besitzen. Wir untersuchen eine rechteckige Potentialbarriere, die auch entweder im Ort oder in der Stärke schwingt. Die Eigenzustände des FWS Operators haben in allen Fällen Eigenschaften, die wünschenswert für das Mikromanipulieren von periodisch schwingenden Objekten sind. Da diese Zustände eine starke Verbindung zu ihren GWS Gegenstücken haben, können wir ihre jeweiligen Eigenschaften leicht interpretieren.

Contents

Abstract ii

Kurzzusammenfassung ii

Contents iii

1. Introduction 1

2. Floquet Scattering Theory 3
2.1. Hamiltonian, Symmetries and Eigenstates 3
2.2. Scattering Properties 7

3. The Generalized Wigner-Smith Operator 10

4. FWS Operator for Oscillating Dirac Delta Potentials 12
4.1. Dirac Delta Potential Oscillating in Space 12
4.2. Dirac Delta Potential Oscillating in Strength 21

5. FWS Operator for Oscillating Barrier Potentials 25
5.1. Barrier Potential Oscillating in Space 25
5.2. Barrier Potential Oscillating in Strength 32

6. Conclusion and Outlook 39

A. Choosing a Proper Cutoff 41

B. Derivation of Eq. (42) 43

C. Numerics concerning Eq. (47) 44

D. Derivation of Eq. (68) 46

Acknowledgements 47

References 48

1. Introduction

Controlling and manipulating small objects with waves is the essence of various physical tools with applications, for example in medicine and biology [1, 2]. Therefore, being able to understand and exploit the behaviour of wave scattering is of great interest. A promising approach in this regard using the advantages of wave control is the generalized Wigner-Smith operator (GWS). The GWS operator was proposed lately in [3] and is based on concepts introduced by Wigner [4] and Smith [5] more than 60 years ago. The power of the GWS theory has very recently been demonstrated theoretically and experimentally in a static microwave setup [6]. The key object in this time-independent protocol is the scattering matrix – connecting incoming and outgoing modes at the same frequency – which is then used to set up the GWS operator. The eigenstates of the GWS operator are shown to be optimal for micromanipulating small objects. Extending this framework into the realm of time-dependent systems is of great interest. First steps have been made using a "frozen scattering matrix" approach [7], where one could show that cooling an ensemble of particles can be realized using a GWS approach. However, this technique is only applicable for slow particles where a quasi-stationary, adiabatic description is valid. Clearly this imposes constrains, especially for in-situ applications. Thus, there is major interest to lift this constraint and exploit the full potential of the additional time parameter by looking at a fully time-dependent description. A first step is presented in this thesis by studying time-periodic systems in which the time dependence can be incorporated without any approximation. Even though energy is in general not conserved anymore in case of time-dependent potentials, the scattering matrix in Floquet theory is unitary and time-independent. This enables us to extend the GWS operator concept in a straightforward way thus introducing the Floquet Wigner-Smith (FWS) operator. Due to the similar structure of the GWS operator and the FWS operator we find analytic expressions for the eigenvalues of the FWS operator, where the corresponding eigenstates feature in general now multiple frequency components and are thus usually pulsed.

We start by introducing the theoretical framework of describing periodically moving objects and their scattering properties – the so-called Floquet scattering theory – in Section 2. In this thesis, we choose to build up our theory for electrons described by the time-dependent Schrödinger equation. This is done, because, historically many investigations focused on the scattering of electrons at periodically moving potentials. Note that the presented concepts based on the Schrödinger equation can be easily transferred into a photonic setup based on the Helmholtz equation. We discuss the main consequences of dealing with a time-periodic Hamiltonian and its implications for the scattering matrix. We then summarize the main concepts of the GWS operator and introduce the novel FWS operator in Section 3. There, we find a strict relation between the eigenvalues of the FWS operator and the absolute value squared of the wavefunction inside the scattering region. This enables one to connect the eigenvalues of the FWS operator with local properties of the wavefunction inside the scattering region. In Sections 4 and 5 we apply the new Floquet concept to specific potentials. In particular, in Section 4 we study

the case of electrons scattering off a Dirac delta potential either oscillating in strength or position. We choose to start with Dirac delta potentials since the interaction regions for such potentials are just a single point in space and therefore its scattering properties are easy to handle. We proceed by examining in Section 5 a more realistic setup of an extended barrier potential – again oscillating in strength or position. We show for all of our examples that the eigenstates of the FWS operator develop exciting properties for the micromanipulation of periodically moving objects.

2. Floquet Scattering Theory

2.1. Hamiltonian, Symmetries and Eigenstates

We start from the time-dependent Schrödinger equation ($\hbar = 1$)

$$H(t)\,|\Phi\rangle = i\frac{\partial}{\partial t}\,|\Phi\rangle\,, \tag{1}$$

where $H(t) = H(t+T)$ is a Hermitian Hamiltonian periodic in time with period $T = 2\pi/\omega$. The Hamiltonian can be separated into the time-independent kinetic energy term and the real, time-periodic potential, i.e.,

$$H(t) = \frac{p^2}{2m} + V(t), \tag{2}$$

with $V(t) = V(t+T)$. In this work we focus on two different kinds of oscillations: potentials oscillating in their amplitude [8, 9] as well as lateral oscillations of their position [10]. Since the system is time-dependent the total energy is not conserved. Nevertheless, the periodicity of the potential induces a conserved quantity: the quasienergy ϵ. In the following we summarize the connection between the Hamiltonian, the time evolution operator $U(t, t_0)$ and the quasienergy. We closely follow the discussions presented in [11–13].

Since the Hamiltonian is Hermitian, the probability is conserved in the system [14], which induces a unitary time evolution operator [15]. The time evolution operator transforms a state from time t_0 to t

$$|\Phi(t)\rangle = U(t, t_0)\,|\Phi(t_0)\rangle\,, \tag{3}$$

which in general involves a time-ordered exponential [16]. The time evolution operator itself satisfies a Schrödinger-like equation

$$i\frac{\mathrm{d}}{\mathrm{d}t}U(t, t_0) = H(t)U(t, t_0), \tag{4}$$

$$U(t_0, t_0) = 1. \tag{5}$$

Furthermore, since

$$U(t_2, t_1)\,|\Phi(t_1)\rangle = U(t_2, t_1)U(t_1, t_0)\,|\Phi(t_0)\rangle = U(t_2, t_0)\,|\Phi(t_0)\rangle\,, \tag{6}$$

it holds that

$$U(t_2, t_0) = U(t_2, t_1)U(t_1, t_0). \tag{7}$$

We now can make use of the fact that the Hamiltonian is periodic in time and derive some helpful results. Following the approach of [17], we first insert $U(t + nT, t_0 + nT)$ into Eq. (4), which leads to

$$i\frac{\mathrm{d}}{\mathrm{d}t}U(t + nT, t_0 + nT) = H(t + nT)U(t + nT, t_0 + nT) \tag{8}$$

$$= H(t)U(t + nT, t_0 + nT), \tag{9}$$

where we used the periodicity of the Hamiltonian. Since $U(t, t_0)$ satisfies the same differential equation and the same initial condition as $U(t + nT, t_0 + nT)$, it holds that

$$U(t + nT, t_0 + nT) = U(t, t_0). \tag{10}$$

Next, we consider the time evolution from an initial time $t = t_0$ to some later time $t = t_0 + nT$, i.e.,

$$\begin{aligned} U(t_0 + nT, t_0) &= U[t_0 + nT, t_0 + (n-1)T] \times \cdots \times U(t_0 + T, t_0) \\ &= U(t_0 + T, t_0) \times \cdots \times U(t_0 + T, t_0) \\ &= [U(t_0 + T, t_0)]^n , \end{aligned} \tag{11}$$

where we used Eq. (7) in the first line and Eq. (10) in the second line. This result proves that propagating by an integer number of periods is equal to the repeated action of the one-period time evolution operator. Finally, by using Eqs. (7) and (11) we observe

$$\begin{aligned} U(t + nT, t_0) &= U(t + nT, t_0 + nT)U(t_0 + nT, t_0) \\ &= U(t, t_0) \left[U(t_0 + T, t_0)\right]^n . \end{aligned} \tag{12}$$

This result reflects a crucial point in the theory of Floquet dynamics: it is sufficient to know $U(t, t_0)$ for $t_0 \leq t \leq T$ in order to construct $U(t, t_0)$ for all times $t \geq t_0$ [12]. Let now $|\Phi_T(t)\rangle$ be an eigenstate of the one-period time evolution operator $U(t + T, t)$,

$$U(t + T, t) \left|\Phi_T(t)\right\rangle = \lambda_T(t) \left|\Phi_T(t)\right\rangle . \tag{13}$$

To show that the eigenvalues $\lambda_T(t)$ of the one-period time evolution operator are actually time-independent, i.e., $\lambda_T(t) = \lambda_T = \text{const.}$, and therefore conserved, we follow the derivation presented in [11]. We use Eqs. (7) and (10) to rewrite the above definition as

$$\begin{aligned} \lambda_T(t) \left|\Phi_T(t)\right\rangle &= U(t + T, t' + T)U(t' + T, t')U(t', t) \left|\Phi_T(t)\right\rangle \\ &= U(t, t')U(t' + T, t')U(t', t) \left|\Phi_T(t)\right\rangle . \end{aligned} \tag{14}$$

Applying $U(t', t)$ from the left on both sides gives

$$\lambda_T(t)U(t', t) \left|\Phi_T(t)\right\rangle = U(t' + T, t')U(t', t) \left|\Phi_T(t)\right\rangle , \tag{15}$$

$$\lambda_T(t) \left|\Phi_T(t')\right\rangle = U(t' + T, t') \left|\Phi_T(t')\right\rangle . \tag{16}$$

This means that if $|\Phi_T(t)\rangle$ is the eigenstate of $U(t + T, t)$ with eigenvalue $\lambda_T(t)$, then for any time t', $|\Phi_T(t')\rangle$ is eigenstate of $U(t' + T, t')$ with the same eigenvalue $\lambda_T(t)$. Therefore, the eigenvalues of $U(t + T, t)$ must be constant and its eigenvectors evolve in time according to $U(t, t_0)$. Since U is a unitary operator its eigenvalues lie on the complex unit circle and we will write

$$\lambda_T = e^{-i\epsilon T}, \tag{17}$$

$$|\Phi_T(t)\rangle \equiv |\Phi_\epsilon(t)\rangle . \tag{18}$$

Here we introduced the quasienergy ϵ. We will discuss its physical implications after defining the so-called Floquet modes.

The Floquet theorem ensures the periodicity of the time-dependent Floquet modes $|\phi_\epsilon(t)\rangle = |\phi_\epsilon(t+T)\rangle$, which are defined with respect to the Floquet state $|\Phi_\epsilon(t)\rangle$ as

$$|\Phi_\epsilon(t)\rangle = e^{-i\epsilon t} |\phi_\epsilon(t)\rangle . \tag{19}$$

Note that only the Floquet states $|\Phi_\epsilon(t)\rangle$ are solutions of the time-dependent Schrödinger equation. Nevertheless, the Floquet modes $|\phi_\epsilon(t)\rangle$ are eigenstates of a Hermitian operator, which we will exploit later. The periodicity of the Floquet modes can be understood by the following argument. We use the eigenvalue equation Eq. (17) and Eq. (19) to write

$$|\Phi_\epsilon(t+T)\rangle = U(t+T,t) |\Phi_\epsilon(t)\rangle = e^{-i\epsilon T} |\Phi_\epsilon(t)\rangle = e^{-i\epsilon T} e^{-i\epsilon t} |\phi_\epsilon(t)\rangle , \tag{20}$$

$$|\Phi_\epsilon(t+T)\rangle = e^{-i\epsilon(t+T)} |\phi_\epsilon(t+T)\rangle = e^{-i\epsilon T} e^{-i\epsilon t} |\phi_\epsilon(t+T)\rangle . \tag{21}$$

Since both lines must hold for any time t, the Floquet modes $|\phi_\epsilon(t)\rangle$ must possess the same periodicity as the Hamiltonian and since $|\Phi_\epsilon(t)|^2 = |\phi_\epsilon(t)|^2$ the probability density is also time-periodic. Because of the periodicity, we can Fourier expand these modes as

$$|\phi_\epsilon(t)\rangle = \sum_n e^{-in\omega t} |\psi_\epsilon^n\rangle , \tag{22}$$

where n is sometimes referred to as the Floquet channel [10]. Summarizing, we can write the Floquet state in the Fourier basis as

$$|\Phi_\epsilon(t)\rangle = \sum_n e^{-i(n\omega+\epsilon)t} |\psi_\epsilon^n\rangle . \tag{23}$$

Coming back to the quasienergy ϵ we observe that Eq. (13) does not define the quasienergy uniquely, since

$$e^{-i(\epsilon+m\omega)T} = e^{-i\epsilon T} = \lambda_T \tag{24}$$

for any integer m, where we used that $T = 2\pi/\omega$. There is a similar redundancy concerning the states. We observe that we can write the eigenstate of $U(t+T,t)$ from Eq. (19) as

$$\begin{aligned} |\Phi_\epsilon(t)\rangle &= e^{-i\epsilon t} \sum_n e^{-in\omega t} |\psi_\epsilon^n\rangle \\ &= e^{-i(\epsilon+m\omega)t} \sum_n e^{-i(n-m)\omega t} |\psi_\epsilon^n\rangle \\ &= e^{-i(\epsilon+m\omega)t} \sum_n e^{-in\omega t} \left|\psi_\epsilon^{n+m}\right\rangle \end{aligned} \tag{25}$$

Furthermore, a state with quasienergy $\epsilon + m\omega$ reads in the Fourier basis as follows

$$|\Phi_{\epsilon+m\omega}(t)\rangle = e^{-i(\epsilon+m\omega)t} \sum_n e^{-in\omega t} \left|\psi_{\epsilon+m\omega}^n\right\rangle . \tag{26}$$

However, since $U(t+T,t)$ is non degenerate and $|\Phi_\epsilon(t)\rangle$ and $|\Phi_{\epsilon+m\omega}(t)\rangle$ have the same eigenvalue, they denote the same eigenstate. Therefore, it holds that

$$\left|\psi^n_{\epsilon+m\omega}\right\rangle = \left|\psi^{n+m}_{\epsilon}\right\rangle . \tag{27}$$

Since there is an equivalence between Floquet states whose quasienergies differ by an integer multiple of ω, we can restrict ourselves to states within a particular interval of ϵ with size ω (like the Bloch theorem enables one to restricts the wavevector to the first Brillouin zone in spatially periodic potential). We make the common choice $0 < \epsilon < \omega$, which we will use throughout this thesis.

As already mentioned above, the Floquet modes themselves satisfy an eigenvalue equation

$$\mathcal{H}\,|\phi_\epsilon(t)\rangle = \epsilon\,|\phi_\epsilon(t)\rangle\,, \tag{28}$$

with the Hermitian operator $\mathcal{H} = H - i\frac{\partial}{\partial t}$ [18, 19]. Since they are eigenfuctions of a Hermitian operator, they form a complete, orthonormal basis set of the composite Hilbert space $\mathcal{F} = \mathcal{R} \otimes \mathcal{T}$. Here $\mathcal{R}$ is the Hilbert space of square integrable functions $\xi_\epsilon(x)$ on configuration space with the inner product defined as

$$\langle \xi_{\epsilon_1+n\omega} | \xi_{\epsilon_2+m\omega} \rangle = \int \mathrm{d}x\, \xi^*_{\epsilon_1+n\omega}(x) \xi_{\epsilon_2+m\omega}(x). \tag{29}$$

Here, the asterisk stands for complex conjugation. On the space $\mathcal{T}$ of functions which are periodic in t with period T the inner product is defined as [13]

$$(m,n) = \frac{1}{T}\int_0^T \mathrm{d}t\, e^{i(n-m)\omega t}. \tag{30}$$

Therefore, the inner product on the composite Hilbert space $\mathcal{F}$ may be defined as

$$\langle\langle \phi_{\epsilon_1+n\omega}(t) | \phi_{\epsilon_2+m\omega}(t) \rangle\rangle = \frac{1}{T}\int_0^T \int \mathrm{d}t\, \mathrm{d}x\, \phi^*_{\epsilon_1+n\omega}(x,t) \phi_{\epsilon_2+m\omega}(x,t). \tag{31}$$

The double bracket symbol introduced here, indicates the inner product used in the Floquet formalism [13, 17, 18]. As one can see, this is a time averaged version of the standard spatial inner product known from quantum mechanics.

2.2. Scattering Properties

Having presented the main theoretical aspects of time-periodic Hamiltonians and Floquet states in the last section, we now summarize their scattering properties. Here we discuss the general characteristics of describing scattering off a time-periodic potential and introduce the Floquet scattering matrix, which will be the key ingredient in formulating a Floquet Wigner-Smith theory.

In this work, we deal with 1D-potentials, which are localized in space. This means that there always exist (asymptotic) potential-free regions, i.e.,

$$V(x) = \begin{cases} 0 & x < -x_1, \\ W(x) & -x_1 < x < x_1, \\ 0 & x > x_1. \end{cases} \tag{32}$$

More specifically, we have $x_1 = L/2$ for the potential barrier and $x_1 = 0$ for the Dirac delta potential. Therefore, we can always divide the space into at most three regions. The potential-free regions I ($x < -x_1$) and III ($x > x_1$) and the interaction region II ($-x_1 < x < x_1$). Note, that for the Dirac delta potential the interaction region is just a single point in space and therefore region II vanishes. In the potential-free regions we can make a flux-normalized plane wave ansatz. The form of the wavefunction inside the scattering region depends on the specific potential $W(x)$. In general, a typical Floquet ansatz for localized potentials is given by

$$\Phi_\epsilon(x,t) = \sum_{n=-\infty}^{\infty} \psi_n(x) e^{-i(\epsilon+n\omega)t}, \tag{33}$$

with

$$\psi_n(x) = \begin{cases} \psi_n^{(I)}(x) & x < -x_1, \\ \psi_n^{(II)}(x) & -x_1 < x < x_1, \\ \psi_n^{(III)}(x) & x > x_1, \end{cases} \tag{34}$$

$$= \begin{cases} \frac{1}{\sqrt{k_n}} \left(a_n e^{ik_n x} + d_n e^{-ik_n x} \right) & x < -x_1, \\ \psi_n^{(II)}(x) & -x_1 < x < x_1, \\ \frac{1}{\sqrt{k_n}} \left(c_n e^{ik_n x} + b_n e^{-ik_n x} \right) & x > x_1. \end{cases} \tag{35}$$

The asymptotic wavevector is defined as

$$k_n = \sqrt{2\mu\,(\epsilon + n\omega)}. \tag{36}$$

Note that for reasons of readability, we adapted the notation from Eq. (22) as $\langle x|\psi_\epsilon^n\rangle = \psi_\epsilon^n(x) \to \psi_n(x)$. We keep this convention throughout the work. The coefficients a_n and b_n (c_n and d_n) are the incoming (outgoing) amplitudes of the corresponding Floquet modes in the Fourier basis $\psi_n(x)$ scattering off the potential. A sketch of such a setting

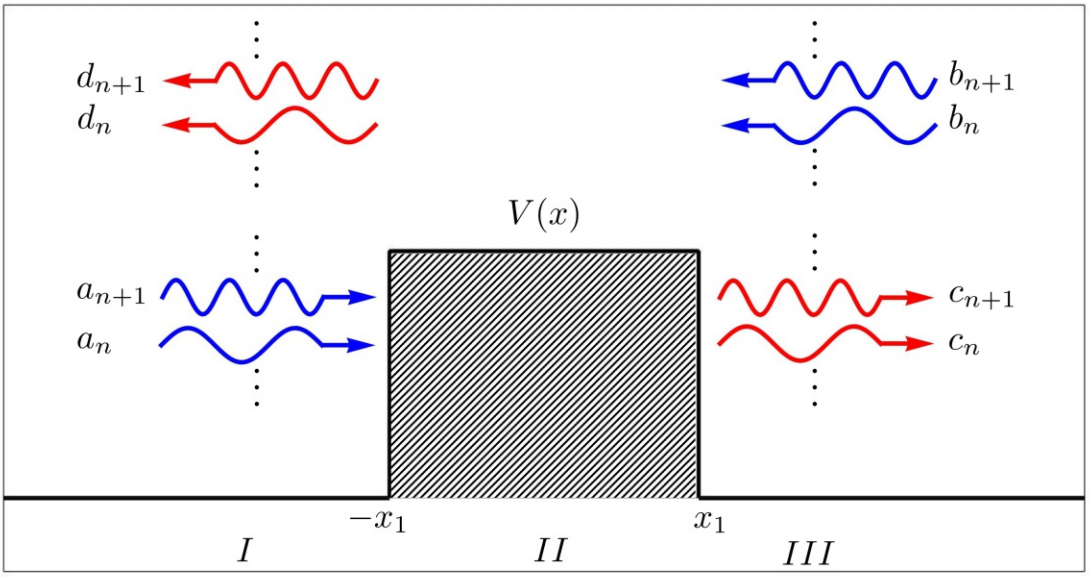

Figure 1: Sketch of a typical setting we focus on in this thesis: a 1D potential, which is localized in space. Therefore, one can divide the space into at most 3 regions, i.e., the asymptotic free regions I and III and the interaction region II. The incoming (blue) and outgoing (red) Floquet coefficients in the asymptotic regions are also indicated.

is depicted in Fig. 1. In the following sections the time-periodic probability density $|\Phi_\epsilon(x,t)|^2 = |\phi_\epsilon(x,t)|^2$ will be studied in order to investigate the properties of various Floquet states.

Modes corresponding to a negative n represent evanescent modes, since in this case the wavevector is purely imaginary (we use the convention $0 < \epsilon < \omega$). Since the wavefunction must be finite everywhere, it holds that there cannot exist incoming evanescent modes, i.e., $a_{n<0} = b_{n<0} = 0$. Thus, evanescent modes are non-propagating and exponentially damped solutions.

With the above ansatz we impose two kinds of normalizations. As mentioned before, we use flux-normalized states in order to get a unitary and flux-conserving Floquet scattering matrix. Additionally, we also demand an intensity normalization, i.e.,

$$\sum_{n\geq 0} |a_n|^2 + |b_n|^2 = 1. \tag{37}$$

One now can define a generalized scattering matrix σ in the Floquet mode basis that connects all incoming with all outgoing mode coefficients (including contributions from evanescent modes), i.e.,

$$\begin{pmatrix} \boldsymbol{d} \\ \boldsymbol{c} \end{pmatrix} = \sigma \begin{pmatrix} \boldsymbol{a} \\ \boldsymbol{b} \end{pmatrix}. \tag{38}$$

Here, $\boldsymbol{a} = (\dots a_{-1}, a_0, a_1 \dots)^T$ is the vector of Floquet mode coefficients, where negative integer subscripts correspond to evanescent modes. Note that σ is not a unitary matrix. However, keeping only entries that connect contributions from propagating modes and neglecting those corresponding to evanescent modes then results in the object we are interested in – the unitary Floquet scattering matrix S. It transforms incoming, asymptotically free, propagating states into propagating, outgoing ones

$$\begin{pmatrix} \boldsymbol{d_p} \\ \boldsymbol{c_p} \end{pmatrix} = S \begin{pmatrix} \boldsymbol{a_p} \\ \boldsymbol{b_p} \end{pmatrix}, \tag{39}$$

where the subscript indicates that we deal with vectors of the form $\boldsymbol{a_p} = (a_0, a_1 \dots)^T$, which now only contain coefficients of propagating modes with $n \geq 0$. It is important to note that – in contrast to static scattering systems – the scattering matrix in the time-periodic case does not only connect states with identical energy but also states with an energy difference of $\Delta E = m\,\omega$, where m is the net number of gained or lost quanta (photons) during the process. Such processes would be called inelastic in a static scattering system, since they violate energy conservation. In the framework of Floquet scattering, however, they can be seen as perfectly elastic since the quasienergy is conserved [20]. Describing multiphoton processes without any approximation is one of the main advantages of Floquet theory. Since the Hamiltonian is Hermitian, the probability(-flux) is conserved. The conservation of flux implies that the Floquet scattering matrix – connecting flux-carrying propagating modes – is a unitary matrix. Furthermore, it holds that $S = S^T$, which is a consequence of the reciprocity of the potential [21].

Nevertheless, for computational reasons, one has to truncate to a finite number of modes, i.e., one has to cut the sum in Eq. (33) as $\sum_{n=-\infty}^{\infty} \to \sum_{n=-\nu_{\text{cut}}}^{n_{\text{cut}}}$, where $n_{\text{cut}} + 1$ is now the truncated number of propagating modes and ν_{cut} the number of evanescent modes. This unavoidably leads to the fact that processes where a mode $n \leq n_{\text{cut}}$ scatters into a mode $n' > n_{\text{cut}}$ cannot be described by the truncated scattering matrix. To approximately maintain the above properties (unitarity and transposition symmetry), one has to be careful in choosing a proper cutoff. Details on the criterion for the cutoff used for the numerics in this work can be found in Appendix A.

3. The Generalized Wigner-Smith Operator

In this section, we first review the main ideas of the generalized Wigner-Smith operator for static scattering systems. There the scattering can be described by a unitary scattering matrix. Since time-periodic systems also feature a unitary and time-independent Floquet scattering matrix, a straightforward way of defining a Floquet Wigner-Smith formalism is presented.

Wigner [4] and Smith [5] first introduced the time delay operator for static scattering

$$\tilde{Q} = -i\tilde{S}^{\dagger}\frac{\mathrm{d}\tilde{S}}{\mathrm{d}\Omega}, \tag{40}$$

where Ω is the energy ($\hbar = 1$) of the incoming particle and $\tilde{S}$ is the static scattering matrix. Note, that we use a tilde in the above expressions corresponding to a static scattering system in order to distinguish them from their time-periodic counterparts. Wigner and his student Eisenbud first formulated this idea of a particle's time-delay due to scattering off a potential in the framework of nuclear scattering and Smith then extended this result to multichannel transport. With their works they could answer the question of how much time a particle spends inside a potential during a scattering process by observing that the eigenstates of this operator $\tilde{Q}$ – called principal modes – have a well defined time delay associated with its eigenvalues. This time delay can be understood as the time an incident wave accumulates during a scattering process compared to a wave which propagates in free space [21]. One should note, that in the definition of the time delay operator a derivative with respect to energy (frequency) is connected to a notion of its conjugate variable time. Following this observation the authors in [3, 6] generalized the concept of the time delay operator by replacing the frequency derivative with a derivative with respect to an arbitrary parameter α, which can be a global one or a local parameter on which the potential depends parametrically. The resulting so-called generalized Wigner-Smith operator is given by

$$\tilde{Q}_{\alpha} = -i\tilde{S}^{\dagger}\frac{\mathrm{d}\tilde{S}}{\mathrm{d}\alpha}. \tag{41}$$

Its eigenvalues are connected to the quantity conjugate to α, where it has been shown that, e.g., choosing α as the spatial position of a scatterer results in eigenvalues which are related to the applied force, i.e., the momentum transferred to it [6]. One can summarize the results for the static case in a single equation

$$\langle\zeta|\tilde{Q}_{\alpha}|\zeta\rangle = -\mu\,\langle\chi_{\zeta}|\frac{\mathrm{d}\tilde{V}(x,\alpha)}{\mathrm{d}\alpha}|\chi_{\zeta}\rangle\,, \tag{42}$$

where $|\zeta\rangle$ is an asymptotic state, $|\chi_{\zeta}\rangle$ is the wavefunction inside the scattering system, μ is the mass of the particle and $\tilde{V}(x,\alpha)$ is the static scattering potential. A sketch of the derivation of Eq. (42) is given in the Appendix B, a detailed version for the photonic case based on the scalar Helmholtz equation can be found in [22] or in the supplementary of [6]. If $|\zeta\rangle$ is chosen to be an eigenstate of the GWS operator, one gets the desired

connection between an eigenvalue $\tilde{\theta}_\alpha$ and local properties inside the scattering region, i.e.,

$$\tilde{\theta}_\alpha = -\mu \langle \chi_\zeta | \frac{\mathrm{d}\tilde{V}(x,\alpha)}{\mathrm{d}\alpha} | \chi_\zeta \rangle \,. \tag{43}$$

Now, we extend the latter formalism of a static scattering system into the realm of time-periodic systems. Similar to the static system, using the unitary Floquet scattering matrix S now allows us to define a Floquet Wigner-Smith (FWS) operator

$$Q_\alpha = -iS^\dagger \frac{\mathrm{d}S}{\mathrm{d}\alpha}. \tag{44}$$

The unitarity of S implies that Q_α possesses real eigenvalues. Assuming that the effective Hamiltonian formalism [23] is also valid in time-periodic system and using the inner product of the Floquet formalism (see Section 2.1) we generalize Eq. (42) as

$$\langle\langle \zeta | Q_\alpha | \zeta \rangle\rangle = \langle\langle \zeta | \frac{\mathrm{d}V(x,t,\alpha)}{\mathrm{d}\alpha} | \zeta \rangle\rangle \tag{45}$$

$$= -\mu \frac{1}{T} \int_0^T \mathrm{d}t \, \langle \chi_\zeta | \frac{\mathrm{d}V(x,t,\alpha)}{\mathrm{d}\alpha} | \chi_\zeta \rangle \,, \tag{46}$$

which again reduces for the case of $|\zeta\rangle$ being an eigenstate of Q_α to

$$\theta_\alpha = -\mu \frac{1}{T} \int_0^T \mathrm{d}t \, \langle \chi_\zeta | \frac{\mathrm{d}V(x,t,\alpha)}{\mathrm{d}\alpha} | \chi_\zeta \rangle \,. \tag{47}$$

This expression shows that the similar structures of the GWS and FWS operators results in similar expressions for the eigenvalues of these two operators, where for the time-periodic case there is an additional time averaging present due to the inner product in the Floquet formalism [see Eq. (31)].

We want to point out that there exists a structural equivalence between the fundamental equations in scattering of quantum matter waves and classical light fields. More specifically, the former can be described by the stationary Schrödinger equation which can be mapped onto an equation used extensively in the description of classical waves, the scalar Helmholtz equation. Altough, there exist essential differences between both systems [21], the structural similarity allows us to easily transfer the results found in this thesis for the electronic case to the photonic case studied in [6]. The most notable difference we have to consider is a relative sign between those two equations. This means that we have to keep in mind that the most negative FWS eigenvalues in the Schrödinger picture will correspond to the most positive ones in the Helmholtz description.

Now that we have an analytical expression for the FWS eigenvalue available, we can test its validity in numerical simulations, examining various systems and parameters α in the following sections. Additionally, in Appendix C, we present an excellent agreement of Eq. (47) with numerical simulations for all the considered time-periodic systems [1].

[1] One of the main assumptions of this thesis is the validity of the effective Hamiltonian formalism in time-periodic settings. This remains to be proven analytically in the course of future projects, but the remarkable agreement between the eigenvalues and the analytical relations let little room for doubt in that regard (cf. Appendix C).

4. FWS Operator for Oscillating Dirac Delta Potentials

4.1. Dirac Delta Potential Oscillating in Space

We now want to apply the FWS operator to a specific potential and start with a Dirac delta potential oscillating in position. In order to do so, we first have to study its scattering properties and derive the Floquet scattering matrix, where we will closely follow the derivations presented in [24, 25]. The Hamiltonian of this system is given by

$$H = \frac{p^2}{2\mu} + V(x,t), \tag{48}$$

where the time-dependent potential reads

$$V(x,t) = V_0 \delta\left[x - a\cos(\omega t)\right]. \tag{49}$$

Here, $p = -i\frac{\mathrm{d}}{\mathrm{d}x}$ is the momentum operator, $V_0 \in \mathbb{R}$ is the strength of the potential, and μ is the mass of the electron. Furthermore, $a > 0$ is the oscillation amplitude and ω is the frequency of the oscillation of the potential. Since the Hamiltonian is periodic with period $T = 2\pi/\omega$, we can make use of Floquet theory. As an ansatz for the wavefunction we choose flux normalized plane Floquet-waves [compare to Eq. (35), but since the scattering region is just a single point in space at $x = x_0$ we only have the two asymptotic regions], i.e.,

$$\Phi_\epsilon(x,t) = \sum_{n=-\infty}^{\infty} \psi_n(x) e^{-i(\epsilon+n\omega)t}, \tag{50}$$

where

$$\psi_n(x,t) = \begin{cases} \psi_n^L(x) = \frac{1}{\sqrt{k_n}}\left(a_n e^{ik_n x} + d_n e^{-ik_n x}\right) & x < x_0, \\ \psi_n^R(x) = \frac{1}{\sqrt{k_n}}\left(c_n e^{ik_n x} + b_n e^{-ik_n x}\right) & x > x_0. \end{cases} \tag{51}$$

We define $x_0 = x_0(t) = a\cos(\omega t)$. In order to determine the coefficients we demand continuity of the wavefunction, which leads to

$$\Phi_\epsilon(x_0^-, t) = \Phi_\epsilon(x_0^+, t). \tag{52}$$

Furthermore, we integrate the Schrödinger equation

$$H(x,t)\Phi_\epsilon(x,t) = i\frac{\mathrm{d}}{\mathrm{d}t}\Phi_\epsilon(x,t) \tag{53}$$

in an interval $x \in [x_0 - \epsilon, x_0 + \epsilon]$, which in the limit $\epsilon \to 0$ leads to

$$-\frac{1}{2\mu}\lim_{\epsilon\to 0}\int_{x_0-\epsilon}^{x_0+\epsilon} \mathrm{d}x \left[\frac{\mathrm{d}^2}{\mathrm{d}x^2} + V_0\delta(x-x_0)\right]\Phi_\epsilon(x,t) = i\frac{\mathrm{d}}{\mathrm{d}t}\lim_{\epsilon\to 0}\int_{x_0-\epsilon}^{x_0+\epsilon}\mathrm{d}x\ \Phi_\epsilon(x,t), \tag{54}$$

$$-\frac{1}{2\mu}\left[\Phi'_\epsilon(x_0^+,t) - \Phi'_\epsilon(x_0^-,t)\right] + V_0\Phi_\epsilon(x_0) = 0, \tag{55}$$

$$\Phi'_\epsilon(x_0^+,t) - \Phi'_\epsilon(x_0^-,t) = 2V_0\mu\Phi_\epsilon(x_0,t), \tag{56}$$

where the prime denotes the derivative with respect to x. We insert the ansatz for the wavefunction Eq. (51) into Eqs. (53) and (56), multiply both equations with $e^{-im\omega t}$, and finally integrate them from time $t = 0$ to T. There we can make use of the identity

$$\int_0^T \mathrm{d}t\, e^{ika\cos(\omega t) - im\omega t} = T i^m J_m(ka), \tag{57}$$

where $J_m(x)$ are the Bessel functions of the first kind [25]. After truncating to a finite number of states one is left with the following set of coupled equations

$$\begin{aligned}\begin{pmatrix} \boldsymbol{d} \\ \boldsymbol{c} \end{pmatrix} &= \begin{pmatrix} -J^- & J^+ \\ M^- & M^+ + 2\mu V J^+ \end{pmatrix}^{-1} \begin{pmatrix} J^+ & -J^- \\ M^+ & M^- - 2\mu V J^- \end{pmatrix} \begin{pmatrix} \boldsymbol{a} \\ \boldsymbol{b} \end{pmatrix} \\ &= \sigma \begin{pmatrix} \boldsymbol{a} \\ \boldsymbol{b} \end{pmatrix}.\end{aligned} \tag{58}$$

The elements of the submatrices in Eq. (58) are given by

$$\left(J^+\right)_{n,m} = \frac{i^{m+n}}{\sqrt{k_m}} J_{m+n}(k_m a), \tag{59}$$

$$\left(J^-\right)_{n,m} = \frac{i^{m+n}}{\sqrt{k_m}} J_{m+n}(-k_m a), \tag{60}$$

$$\left(M^+\right)_{n,m} = i^{m+n+1}\sqrt{k_m} J_{m+n}(k_m a), \tag{61}$$

$$\left(M^-\right)_{n,m} = i^{m+n+1}\sqrt{k_m} J_{m+n}(-k_m a). \tag{62}$$

Note, that $J_m(0) = \delta_{m,0}$ and thus we recover the static uncoupled case for $a \to 0$ as expected. To get the Floquet matrix we only take entries from σ that connect propagating modes, i.e.

$$\begin{pmatrix} \boldsymbol{d_p} \\ \boldsymbol{c_p} \end{pmatrix} = S \begin{pmatrix} \boldsymbol{a_p} \\ \boldsymbol{b_p} \end{pmatrix}. \tag{63}$$

Having now the unitary Floquet scattering matrix in hands, we can use it to set up various FWS operators.

We start by examining the FWS operator with respect to the strength V_0 of the potential, i.e.

$$Q_{V_0} = -iS^\dagger \frac{\mathrm{d}S}{\mathrm{d}V_0}. \tag{64}$$

According to Eq. (47) for an eigenstate $\Phi_\epsilon(x,t)$ with corresponding eigenvalue θ_{V_0} it holds that

$$\begin{aligned}\theta_{V_0} &= -\mu \frac{1}{T} \int_0^T \mathrm{d}t\, \langle \Phi_\epsilon | \frac{\mathrm{d}V(x,t)}{\mathrm{d}V_0} | \Phi_\epsilon \rangle \\ &= -\mu \frac{1}{T} \int_0^T \mathrm{d}t\, |\Phi_\epsilon[a\cos(\omega t), t]|^2.\end{aligned} \tag{65}$$

We see that the eigenvalues are connected to the probability density right at the (moving) position of the delta potential. In the photonic case this would correspond to the intensity of the light. Therefore, choosing the eigenstate that corresponds to the smallest (most negative) eigenvalue will maximize the probability of finding the electron at the location of the potential $x_0(t)$. This state is depicted in Fig. 2. The wavefunction clearly follows the oscillation of the Dirac delta potential (red line) and forms two local maxima in the immediate vicinity of the delta peak maximizing the probability density at $x_0(t)$. These maxima are separated by a cusp, which is typical for repulsive Dirac delta potentials. This cusp is induced by the jump of the first derivative of the wavefunction [see Eq. (56)]. A

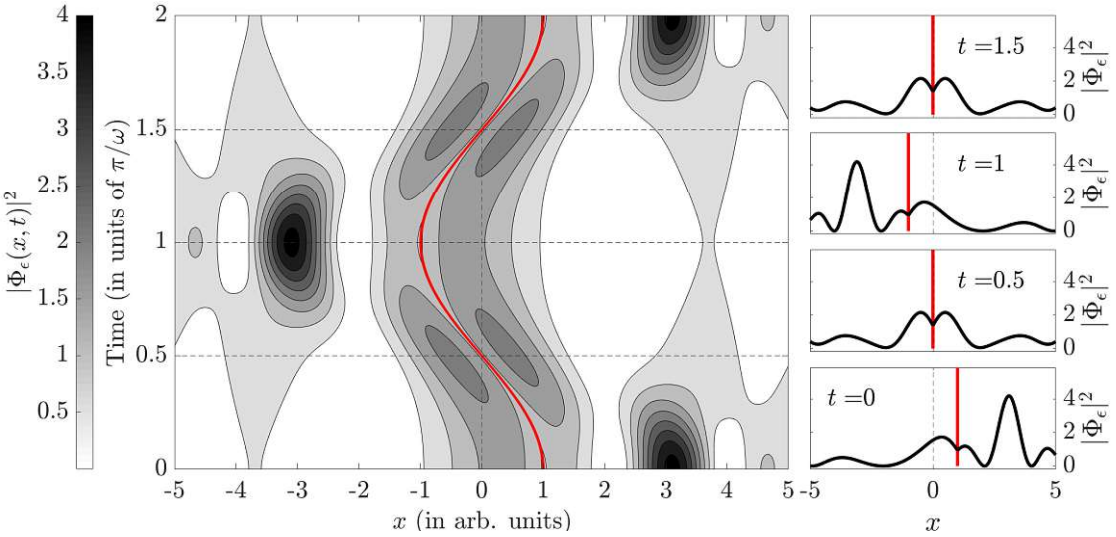

Figure 2: Absolute value of the eigenstate wavefunction $|\Phi_\epsilon(x,t)|^2$ corresponding to the smallest eigenvalue of Q_{V_0} with $V_0 > 0$. This state maximizes the probability of finding the electron at the position of the Dirac delta potential. The right panels are cuts through the contour plot at the specified times. The red line represents the position of the repulsive Dirac delta potential. In this plot the parameters take the values $\mu = 1$, $\omega = 1$, $a = 1$, $V_0 = 1$, $\epsilon = 0.7$ (arb. units).

state corresponding to an eigenvalue close to zero, which is in that case also the maximal eigenvalue possible [cf. Eq. (65)], avoids exhibiting much probability density at the position of the Dirac delta potential at all times such that the probability for finding the electron there is almost zero. For the FWS operator Q_{V_0} there exist many eigenstates corresponding to an eigenvalue close to zero. We show one of these states in Fig. 3. Clearly, this state exhibits a minimum at $x_0(t)$ for all times as expected. In order to emphasize that all of the degenerate states corresponding to an eigenvalue close to zero minimize the probability density at the position of the potential, we show in Fig. 4 a incoherent superposition of ten of these eigenstates. As one can see, there is still a minimum present at the time depended location of the potential as Eq. (65) predicts.

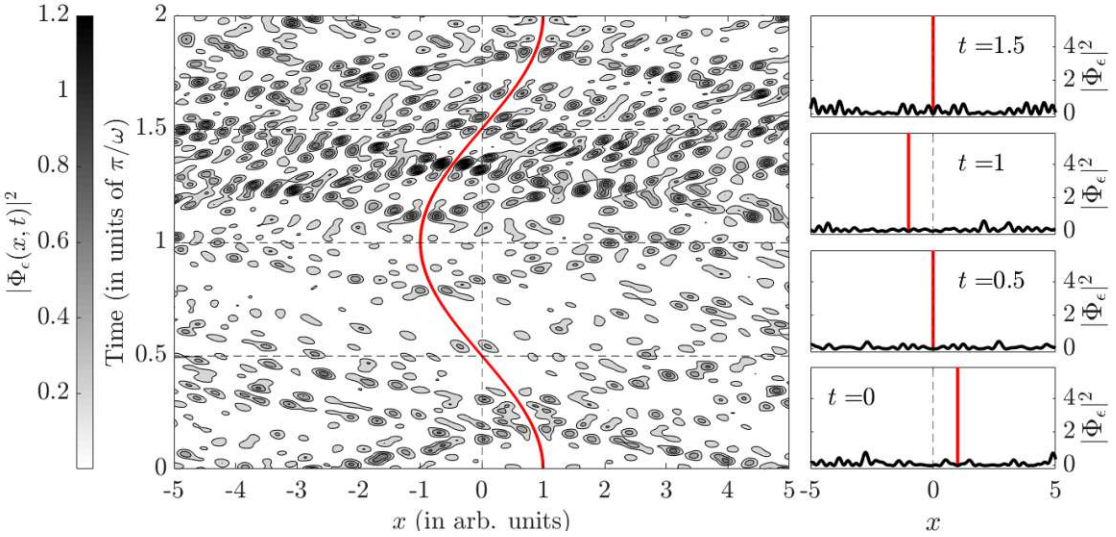

Figure 3: Absolute value of the eigenstate wavefunction $|\Phi_\epsilon(x,t)|^2$ corresponding to an eigenvalue close to zero of Q_{V_0} with $V_0 > 0$. This state minimizes the probability of finding the electron at the position of the Dirac delta potential. The right panels are cuts through the contour plot at the specified times. The red line represents the position of the repulsive Dirac delta potential. In this plot the parameters take the values $\mu = 1$, $\omega = 1$, $a = 1$, $V_0 = 1$, $\epsilon = 0.7$ (arb. units).

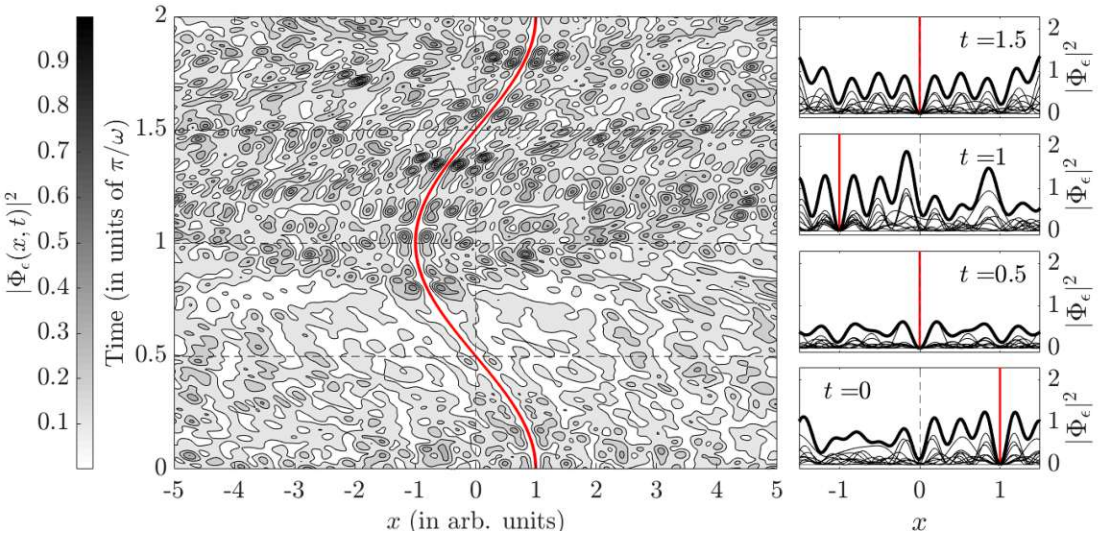

Figure 4: Absolute value of the incoherent superposition of ten eigenstate wavefunctions $|\Phi_\epsilon(x,t)|^2$ corresponding to an eigenvalue close to zero of Q_{V_0} with $V_0 > 0$. The incoherent superposition still minimizes the probability of finding the electron at the position of the Dirac delta potential. The right panels explicitly show the probability density of the states contained in the incoherent superposition (thin black lines) and rescaled cuts through the contour plot (thick black lines) at the specified times. Every state exhibits a minimum at the position of the repulsive Dirac delta potential (red line). In this plot the parameters take the values $\mu = 1$, $\omega = 1$, $a = 1$, $V_0 = 1$, $\epsilon = 0.7$ (arb. units).

In order to gain further insight, we investigate the behaviour of the eigenstate corresponding to the smallest eigenvalue of Q_{V_0} for an attractive Dirac delta potential, i.e., $V_0 < 0$. This state is depicted in Fig. 5. In accordance with Eq. (65) this state again maximizes the probability density at the position of the Dirac delta potential (blue line) at all times. In contrast to the repulsive case, here a local maximum of the probability density is formed right at $x_0(t)$ again resulting in a high probability of finding the electron there.

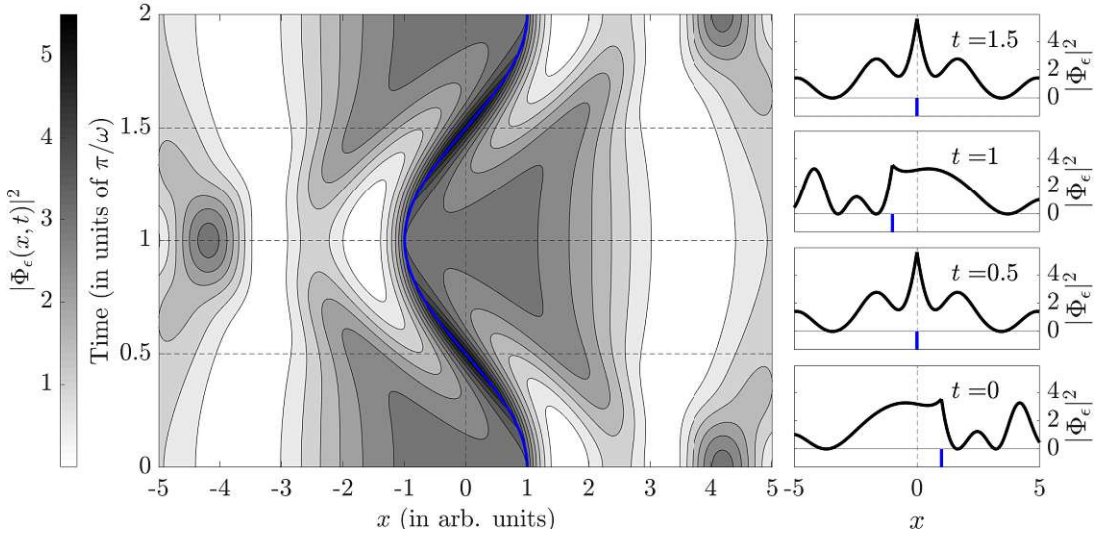

Figure 5: Absolute value of the eigenstate wavefunction $|\Phi_\epsilon(x,t)|^2$ corresponding to the smallest eigenvalue of Q_{V_0} with $V_0 < 0$. This state maximizes the probability of finding the electron at the position of the Dirac delta potential. The right panels are cuts through the contour plot at the specified times. The blue line represents the position of the attractive Dirac delta potential. In this plot the parameters take the values $\mu = 1$, $\omega = 1$, $a = 1$, $V_0 = -1$, $\epsilon = 0.7$ (arb. units).

Furthermore, we want to study the behaviour of eigenstates corresponding to eigenvalues close to zero. Also for an attractive Dirac delta potential Eq. (65) tells us, that these states will minimize the probability density at the time-depended position of the potential. One can evidently observe this behaviour for a single state in Fig. 6 and for an incoherent superposition of ten nearly degenerate eigenstates in Fig. 7.

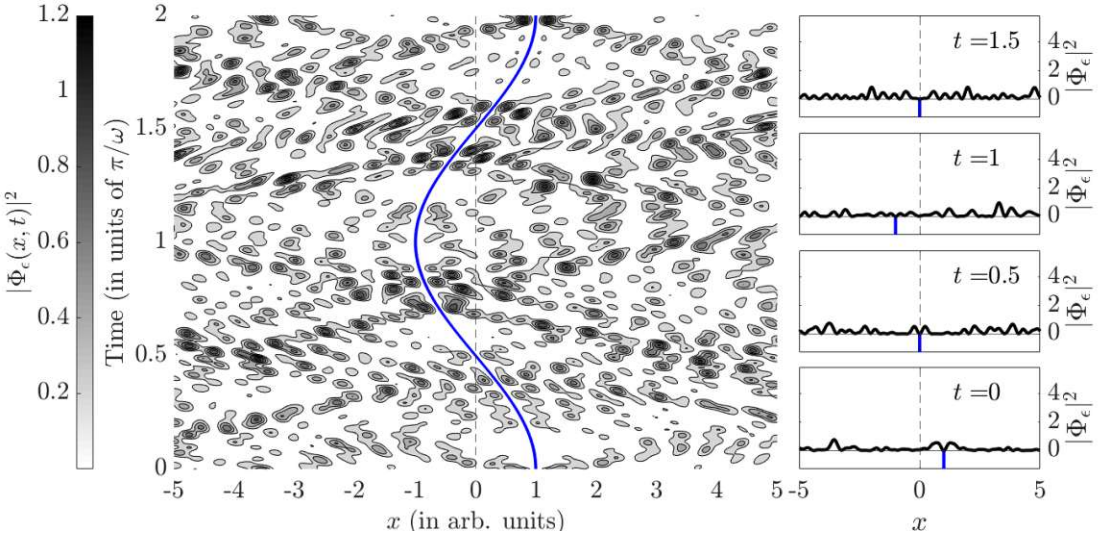

Figure 6: Absolute value of the eigenstate wavefunction $|\Phi_\epsilon(x,t)|^2$ corresponding to an eigenvalue close to zero of Q_{V_0} with $V_0 < 0$. This state minimizes the probability of finding the electron at the position of the Dirac delta potential. The right panels are cuts through the contour plot at the specified times. The blue line represents the position of the repulsive Dirac delta potential. In this plot the parameters take the values $\mu = 1$, $\omega = 1$, $a = 1$, $V_0 = 1$, $\epsilon = 0.7$ (arb. units).

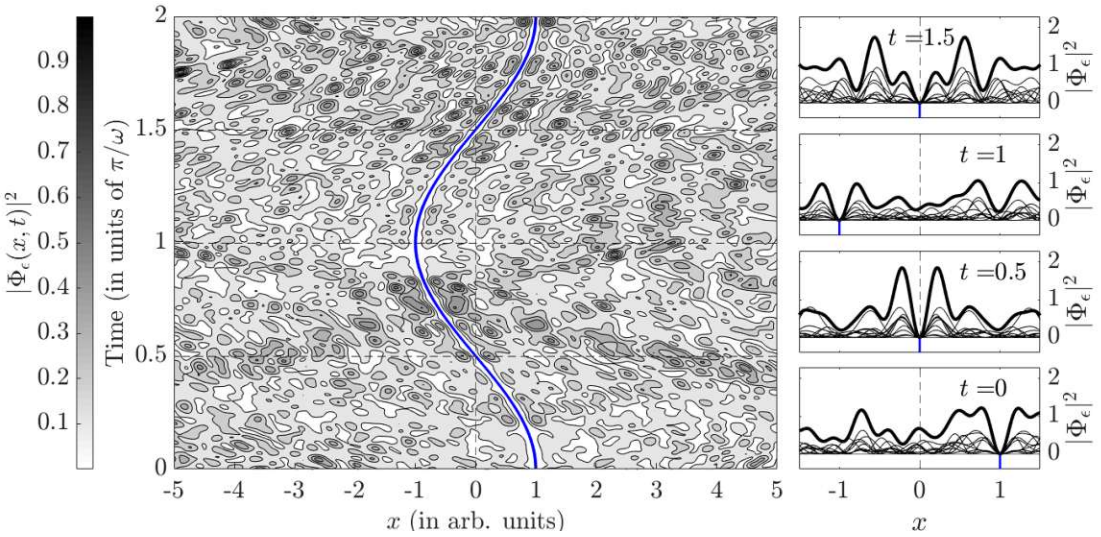

Figure 7: Absolute value of the incoherent superposition of ten eigenstate wavefunctions $|\Phi_\epsilon(x,t)|^2$ corresponding to an eigenvalue close to zero of Q_{V_0} with $V_0 > 0$. The incoherent superposition still minimizes the probability of finding the electron at the position of the Dirac delta potential. The right panels explicitly show the probability density of the states contained in the incoherent superposition (thin black lines) and rescaled cuts through the contour plot (thick black lines) at the specified times. Every state exhibits a minimum at the position of the repulsive Dirac delta potential (blue line). In this plot the parameters take the values $\mu = 1$, $\omega = 1$, $a = 1$, $V_0 = 1$, $\epsilon = 0.7$ (arb. units).

A second FWS operator we want to investigate is the one with a derivative with respect to the amplitude of the oscillation

$$Q_a = -iS^\dagger \frac{\mathrm{d}S}{\mathrm{d}a}. \tag{66}$$

Note, that the above derivative can be rewritten as follows

$$\frac{\mathrm{d}}{\mathrm{d}a} = \frac{\mathrm{d}x_0}{\mathrm{d}a}\frac{\mathrm{d}}{\mathrm{d}x_0} = \cos(\omega t)\frac{\mathrm{d}}{\mathrm{d}x_0}. \tag{67}$$

Due to the appearance of a spatial derivative in Eq. (67), the eigenvalues of this FWS operator are therefore connected to a notion of the conjugate quantity – the momentum, or more specifically the momentum transferred to the potential (this fact was rigorously proven for the static, photonic case in the supplementary material of [6]). We again apply Eq. (47), but are left with an ill-defined expression

$$\begin{aligned}
\theta_a &= -\mu\frac{1}{T}\int_0^T \mathrm{d}t\ \langle\Phi_\epsilon|\frac{\mathrm{d}V(x,t)}{\mathrm{d}a}|\Phi_\epsilon\rangle \\
&= -\mu\frac{V_0}{T}\int_0^T \mathrm{d}t\ \frac{\mathrm{d}}{\mathrm{d}a}|\Phi_\epsilon[a\cos(\omega t),t]|^2 \\
&= -\mu\frac{V_0}{T}\int_0^T \mathrm{d}t\cos(\omega t)\frac{\mathrm{d}}{\mathrm{d}x_0}|\Phi_\epsilon[a\cos(\omega t),t]|^2,
\end{aligned} \tag{68}$$

since the derivative of the wavefunction at the position of the Dirac delta potential is discontinuous. However, we can find a proper expression by considering an extended potential barrier (cf. Section 5.1) and applying the Dirac delta limit, i.e., the spatial extension of the barrier tends to zero and simultaneously the strength tends to infinity such that the product of these parameters stays constant. These considerations result in

$$\begin{aligned}
\theta_a &= -\mu\frac{1}{T}\int_0^T \mathrm{d}t\ \langle\Phi_\epsilon|\frac{\mathrm{d}V(x,t)}{\mathrm{d}a}|\Phi_\epsilon\rangle \\
&= -\mu\frac{V_0}{T}\int_0^T \mathrm{d}t\ \frac{1}{2}\left[\frac{\mathrm{d}}{\mathrm{d}a}\left|\Phi_\epsilon(x_0^-,t)\right|^2 + \frac{\mathrm{d}}{\mathrm{d}a}\left|\psi(x_0^+,t)\right|^2\right] \\
&= -\mu\frac{V_0}{T}\int_0^T \mathrm{d}t\ \frac{1}{2}\cos(\omega t)\left[\frac{\mathrm{d}}{\mathrm{d}x_0}\left|\Phi_\epsilon(x_0^-,t)\right|^2 + \frac{\mathrm{d}}{\mathrm{d}x_0}\left|\Phi_\epsilon\psi(x_0^+,t)\right|^2\right].
\end{aligned} \tag{69}$$

A detailed derivation of this formula can be found in Appendix D. An intuitive way of understanding the action of this FWS operator can be gained by observing the case where V_0 is by far the largest scale of the system. In this case, the strong potential rigorously divides space into the left hand side $x < x_0(t)$ and the right hand side $x > x_0(t)$, such that no information can be transferred between the two parts of the wavefunction – similar to a hard wall. For this set of parameters the eigenstates that correspond to the minimal and maximal eigenvalue exhibit a wavepacket, which hits the potential just at the point of maximal displacement, i.e., at the turning points. More specifically, the

probability of finding the electron right next to the Dirac delta potential is highest at the turning points of the potential. Translating these result to the scalar Helmholtz case would mean that the intensity of the light is highest at the turning points. In Fig. 8 the eigenstate corresponding to the smallest (most negative) eigenvalue is depicted. Since this state corresponds to an extremal eigenvalue, a maximal momentum transfer is associated with it. As can be seen, this state applies a momentum transfer in positive x- direction at times when the cosine weighting factor is minimal (most negative) and momentum transfer in negative x- direction when the weighting factor is maximal (most positive). On the contrary, the eigenstate corresponding to the largest (most positive) eigenvalue hits the potential just from the other side at the turning points of the potential and therefore applying maximal momentum transfer in negative x- direction at times when the cosine weighting factor is minimal and in positive x- direction when the weighting factor is maximal (cf. Fig. 9).

It is also interesting to mention the behaviour of the state corresponding to the eigenvalue close to zero: This state develops two pulses, which hit the potential simultaneously from both sides exactly when the potential is located at $x = 0$ such that almost no momentum gets transferred (not shown).

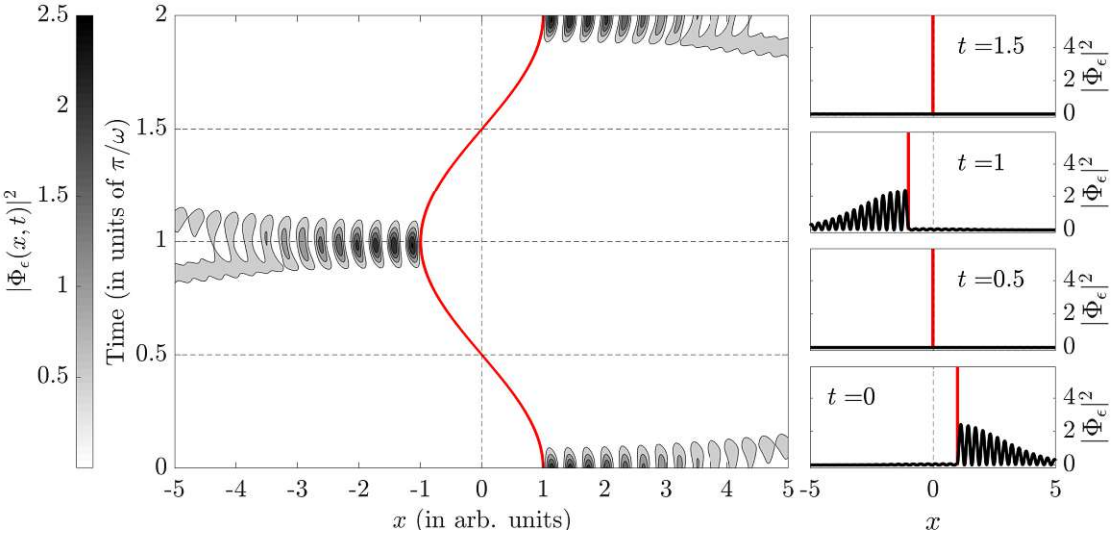

Figure 8: Absolute value of the eigenstate wavefunction $|\Phi_\epsilon(x,t)|^2$ corresponding to the smallest eigenvalue of Q_a. This state hits the potential at the points of maximal displacement, i.e., the turning points, such that there is maximal momentum transfer in positive x- direction. The right panels are cuts through the contour plot at the specified times. The red line represents to position of the Dirac delta potential. In this plot the parameters take the values $\mu = 1$, $\omega = 1$, $a = 1$, $V_0 = 30$, $\epsilon = 0.7$ (arb. units).

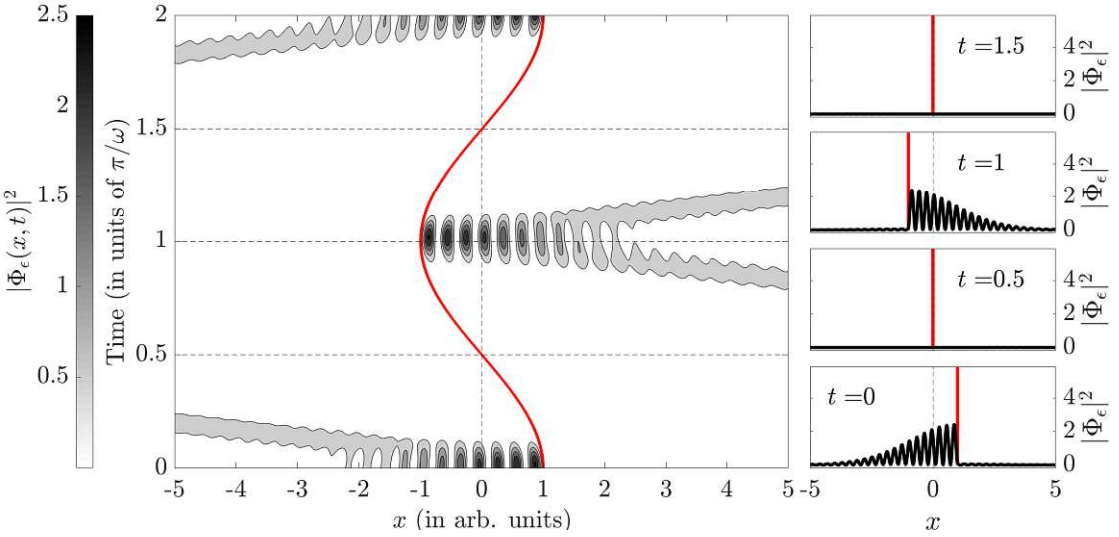

Figure 9: Absolute value of the eigenstate wavefunction $|\Phi_\epsilon(x,t)|^2$ corresponding to the largest eigenvalue of Q_a. This state hits the potential at the points of maximal displacement, i.e., the turning points, such that there is maximal momentum transfer in negative x- direction. The right panels are cuts through the contour plot at the specified times. The red line represents to position of the Dirac delta potential. In this plot the parameters take the values $\mu = 1$, $\omega = 1$, $a = 1$, $V_0 = 30$, $\epsilon = 0.7$ (arb. units).

4.2. Dirac Delta Potential Oscillating in Strength

One can also apply the Floquet Wigner-Smith formalism to a Dirac delta potential not oscillating in position but in strength. In order to derive the Floquet scattering matrix we closely follow the derivations appearing in [8, 26]. The Hamiltonian for this system reads

$$\begin{aligned} H =& \frac{p^2}{2\mu} + V(x,t) \\ =& -\frac{1}{2\mu}\frac{\mathrm{d}^2}{\mathrm{d}x^2} + V_0\cos(\omega t)\delta(x), \end{aligned} \tag{70}$$

where ω is now the characteristic frequency of the potential's oscillation in strength. To calculate the wavefunction we again make the Floquet-ansatz

$$\Phi_\epsilon(x,t) = \sum_{n=-\infty}^{\infty} \psi_n(x) e^{-i(\epsilon+n\omega)t}, \tag{71}$$

where

$$\psi_n(x) = \begin{cases} \psi_n^L(x) = \frac{1}{\sqrt{k_n}}\left(a_n e^{ik_n x} + d_n e^{-ik_n x}\right) & x < 0 \\ \psi_n^R(x) = \frac{1}{\sqrt{k_n}}\left(c_n e^{ik_n x} + b_n e^{-ik_n x}\right) & x > 0 \end{cases}. \tag{72}$$

To determine the coefficients, we again demand the continuity of the wavefunction and the discontinuity of the first derivative [see Eq. (56)]

$$\Phi'_\epsilon(0^+,t) = \Phi'_\epsilon(0^-,t), \tag{73}$$

$$\Phi'_\epsilon(0^+,t) - \Phi'_\epsilon(0^-,t) = 2\mu V_0\cos(\omega t)\Phi_\epsilon(0,t). \tag{74}$$

After inserting the ansatz of the wavefunction, the above equations turn into

$$a_n + d_n = c_n + b_n, \tag{75}$$

$$c_n + d_n - b_n - a_n = -2i\left[h_{n-1}(a_{n-1} + d_{n-1}) + h_n(a_{n+1} + d_{n+1})\right], \tag{76}$$

where the height of the jump of the first derivative is

$$h_n = \frac{\mu V_0}{2\sqrt{k_n k_{n+1}}}. \tag{77}$$

We use vector notation also for evanescent modes as $\boldsymbol{c_e} = (c_{-1}, c_{-2}, \dots)^T$, where the subscript e indicates that we deal with evanescent modes only in contrast to vectors with a subscript p corresponding to propagating modes. One can rewrite Eqs. (75) and (76) as follows

$$\left(1 + X_{pp}\right)\boldsymbol{c_p} + X_{pe}\boldsymbol{c_e} = \boldsymbol{a_p} - X_{pp}\boldsymbol{b_p}, \tag{78}$$

$$X_{ep}\boldsymbol{c_p} + \left(1 + X_{ee}\right)\boldsymbol{c_e} = -X_{ep}\boldsymbol{b_p}, \tag{79}$$

$$\left(1 + X_{pp}\right)\boldsymbol{d_p} + X_{pe}\boldsymbol{d_e} = \boldsymbol{b_p} - X_{pp}\boldsymbol{a_p}, \tag{80}$$

$$X_{ep}\boldsymbol{d_p} + \left(1 + X_{ee}\right)\boldsymbol{d_e} = -X_{ep}\boldsymbol{a_p}. \tag{81}$$

Using the convention $m = 0, 1, \ldots \infty$ and $\nu = -1, -2, \cdots - \infty$, the elements of the matrices appearing in Eqs. (78)- (81) read

$$(\boldsymbol{X_{pp}})_{m,m'} = ih_{m'}\delta_{m,m'+1} + ih_m\delta_{m,m'-1}, \tag{82}$$

$$(\boldsymbol{X_{ee}})_{\nu,\nu'} = ih_{\nu}\delta_{\nu,\nu'-1} + ih_{\nu'}\delta_{\nu,\nu'+1}, \tag{83}$$

$$(\boldsymbol{X_{pe}})_{m,\nu} = ih_{-1}\delta_{m,0}\delta_{\nu,-1}, \tag{84}$$

$$(\boldsymbol{X_{ep}})_{\nu,m} = ih_{-1}\delta_{m,0}\delta_{\nu,-1}. \tag{85}$$

Truncating to a finite number of states and rearranging Eqs. (78)- (81), we are able to identify the Floquet scattering matrix S connecting incoming with outgoing propagating modes

$$\begin{pmatrix} \boldsymbol{d_p} \\ \boldsymbol{c_p} \end{pmatrix} = S \begin{pmatrix} \boldsymbol{a_p} \\ \boldsymbol{b_p} \end{pmatrix}. \tag{86}$$

This enables use to now apply the Floquet Wigner-Smith formalism.

We study the FWS operator with respect to V_0

$$Q_{V_0} = -iS^{\dagger}\frac{\mathrm{d}S}{\mathrm{d}V_0}. \tag{87}$$

Using Eq. (47), we arrive at the following expression for the FWS eigenvalues

$$\begin{aligned} \theta_{V_0} &= -\mu\frac{1}{T}\int_0^T \mathrm{d}t\ \langle\Phi_\epsilon|\frac{\mathrm{d}V(x,t)}{\mathrm{d}V_0}|\Phi_\epsilon\rangle \\ &= -\mu\frac{1}{T}\int_0^T \mathrm{d}t\cos(\omega t)|\Phi_\epsilon(0,t)|^2. \end{aligned} \tag{88}$$

We see, that the eigenvalues θ_{V_0} are connected to the cosine weighted probability density at the position of the Dirac delta potential. Due to the weighting factor, the eigenstates exhibit a probability distribution, which noticeably changes during the duration of one period according to the present value of the weighting factor. To illustrate this behaviour, the eigenstate corresponding to the most negative eigenvalue is depicted in Fig. 10. Indeed, according to Eq. (88), this state maximizes the time average of the cosine weighted probability density at the position of the potential, i.e., $\cos(\omega t)|\psi(0,t)|^2$. One can clearly observe that this state exhibits a large probability density at $x = 0$ about $t = 0$ and $t = 2\pi/\omega$, where the cosine-weight is maximal, i.e., $\cos(0) = 1$. This makes θ_{V_0} as large as possible. We can interpret the behaviour of this state as the one where the probability of finding the electron at the position of the Dirac delta potential is highest when the strength of the potential is positive. Contrary, for the state corresponding the most positive eigenvalue the probability of finding the electron at the potential is largest when the strength is most negative, i.e., at $t = \pi/\omega$ (cf. Fig. 11). It is also interesting to mention the behaviour of an eigenstate corresponding to an eigenvalue close to zero. This state tries to minimize the probability density at the position of the Dirac delta potential at all times by interfering destructively with the input wave from the other side, making it unlikely to ever find the electron at $x = 0$ (not shown).

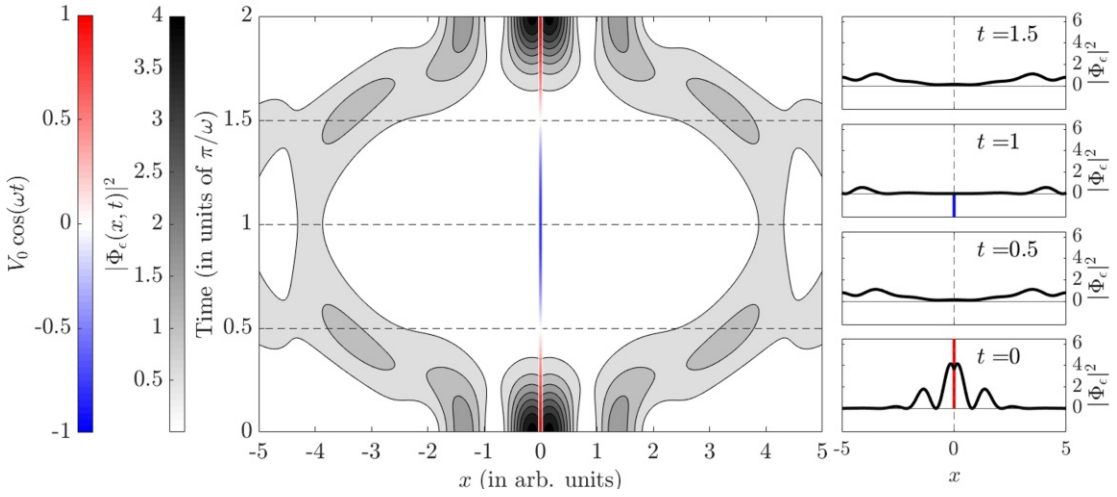

Figure 10: Absolute value of the eigenstate wavefunction $|\Phi_\epsilon(x,t)|^2$ corresponding to the smallest eigenvalue of Q_{V_0} (black to white). For this state the probability of finding the electron at the position of the potential is highest when the strength of the potential is largest. Red to blue color represents the time-dependent strength of the Dirac delta potential. In this plot the parameters take the values $\mu = 1$, $\omega = 1$,$V_0 = 1$, $\epsilon = 0.7$ (arb. units).

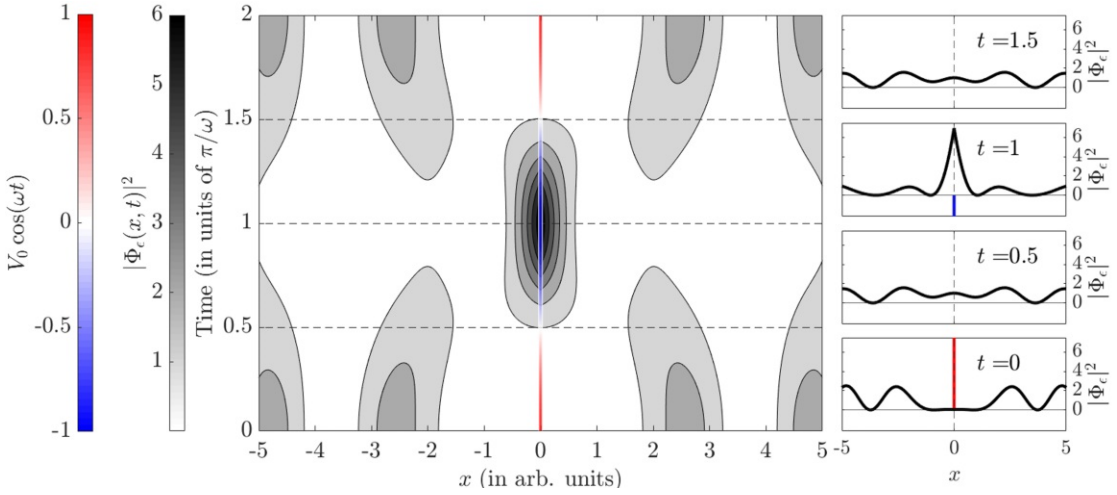

Figure 11: Absolute value of the eigenstate wavefunction $|\Phi_\epsilon(x,t)|^2$ corresponding to the largest eigenvalue of Q_{V_0} (black to white). For this state the probability of finding the electron at the position of the potential is highest when the strength of the potential is smallest. Red to blue color represents the time-dependent strength of the Dirac delta potential. In this plot the parameters take the values $\mu = 1$, $\omega = 1$,$V_0 = 1$, $\epsilon = 0.7$ (arb. units).

Summarizing, we managed to apply the FWS formalism to a Dirac delta potential oscillating in position or in strength. We studied several FWS operators, derived analytical expressions for their eigenvalues, and investigated the temporal behaviour of the corresponding eigenstates which typically consist of multiple Floquet modes with different frequencies thus being wavepackets. However, since a Dirac delta potential is intrinsically singular and therefore non-physical (but can physically be approximated by the limiting case of a potential whose spatial extent is much smaller than the wavelength [27]), we also want to study more realistic potentials, which are extended in space. Therefore, in Section 5 we will apply the FWS formalism to a potential barrier of length $L > 0$.

5. FWS Operator for Oscillating Barrier Potentials

5.1. Barrier Potential Oscillating in Space

First, we investigate a barrier potential whose position oscillates in space. In order to derive the Floquet scattering matrix we again follow the ideas presented in [24, 25]. The potential reads

$$\begin{aligned} V(x,t) &= V_0 \Theta\left(x + L/2 - x_0\right) \Theta\left(L/2 + x_0 - x\right) \\ &= \begin{cases} V_0 & -L/2 + x_0 < x < L/2 + x_0, \\ 0 & \text{else}, \end{cases} \end{aligned} \tag{89}$$

where again $x_0 = x_0(t) = a\cos(\omega t)$ and $\Theta(x)$ is the Heaviside step function. As an ansatz, we take

$$\Phi_\epsilon(x,t) = \sum_{n=-\infty}^{\infty} \psi_n(x,t) e^{-i(\epsilon + n\omega)t}, \tag{90}$$

where for the barrier we now have to distinguish three regions

$$\psi_n(x,t) = \begin{cases} \psi_n^{(I)}(x) & x < -L/2 + x_0, \\ \psi_n^{(II)}(x) & -L/2 + x_0 < x < L/2 + x_0, \\ \psi_n^{(III)}(x) & x > L/2 + x_0, \end{cases} \tag{91}$$

The spatial wavefunctions read

$$\psi_n^{(I)}(x) = \frac{1}{\sqrt{k_n}} \left(a_n e^{ik_n x} + d_n e^{-ik_n x} \right), \tag{92}$$

$$\psi_n^{(II)}(x) = \frac{1}{\sqrt{q_n}} \left(\alpha_n e^{iq_n x} + \beta_n e^{-iq_n x} \right), \tag{93}$$

$$\psi_n^{(III)}(x) = \frac{1}{\sqrt{k_n}} \left(c_n e^{-ik_n x} + b_n e^{ik_n x} \right), \tag{94}$$

where we define the momenta q_n inside the scattering region as

$$q_n = \sqrt{2\mu\left(\epsilon + n\omega - V_0\right)}. \tag{95}$$

We demand continuity of the wavefunction and its first derivative at $x = \pm L/2 + x_0$, which leads – after truncation of the sums – to a set of four coupled equations. Note that we always truncate to the same number of Floquet modes irrespective of the region, i.e., there are as much propagating and evanescent Floquet modes in the interaction region as in the asymptotic regions. From the continuity condition at $x = -L/2 + x_0$ one gets

$$\begin{aligned} &\sum_n \frac{1}{\sqrt{k_n}} \left[a_n e^{ik_n(-L/2)} e^{ik_n a\cos(\omega t)} + d_n e^{-ik_n(-L/2)} e^{-ik_n a\cos(\omega t)} \right] e^{-in\omega t} \\ &= \sum_n \frac{1}{\sqrt{q_n}} \left[\alpha_n e^{iq_n(-L/2)} e^{iq_n a\cos(\omega t)} + \beta_n e^{-iq_n(-L/2)} e^{-iq_n a\cos(\omega t)} \right] e^{-in\omega t}. \end{aligned} \tag{96}$$

We then multiply both sides with $e^{-i\omega m t}$ and integrate over one period in order to get rid of the remaining time-dependence. Here we can again make use of the integral identity Eq. (57), which leads to

$$\begin{aligned}&\sum_n \frac{i^{m+n}}{\sqrt{k_n}}\left[a_n e^{ik_n(-L/2)}J_{m+n}(k_n a)+d_n e^{-ik_n(-L/2)}J_{m+n}(-k_n a)\right]\\&=\sum_n \frac{i^{m+n}}{\sqrt{q_n}}\left[\alpha_n e^{iq_n(-L/2)}J_{m+n}(q_n a)+\beta_n e^{-iq_n(-L/2)}J_{m+n}(-q_n a)\right].\end{aligned} \tag{97}$$

Similarly, we can handle the three remaining sets of equations, which all together leads to

$$L_+^k \boldsymbol{a} + L_-^k \boldsymbol{d} = L_+^q \boldsymbol{\alpha} + L_-^q \boldsymbol{\beta}, \tag{98}$$

$$R_+^q \boldsymbol{\alpha} + R_-^q \boldsymbol{\beta} = R_+^k \boldsymbol{c} + R_-^k \boldsymbol{b}, \tag{99}$$

$$\Lambda_+^k \boldsymbol{a} - \Lambda_-^k \boldsymbol{d} = \Lambda_+^q \boldsymbol{\alpha} - \Lambda_-^q \boldsymbol{\beta}, \tag{100}$$

$$\rho_+^q \boldsymbol{\alpha} - \rho_-^q \boldsymbol{\beta} = \rho_+^k \boldsymbol{c} - \rho_-^k \boldsymbol{b}. \tag{101}$$

The elements of the appearing matrices are given by

$$\left(L_\pm^\gamma\right)_{n,m} = \frac{i^{m+n}}{\sqrt{\gamma_n}} e^{\mp i\gamma_n L/2} J_{n+m}(\pm\gamma_n a), \tag{102}$$

$$\left(R_\pm^\gamma\right)_{n,m} = \frac{i^{m+n}}{\sqrt{\gamma_n}} e^{\pm i\gamma_n L/2} J_{n+m}(\pm\gamma_n a), \tag{103}$$

$$\left(\Lambda_\pm^\gamma\right)_{n,m} = i^{m+n+1}\sqrt{\gamma_n} e^{\mp i\gamma_n L/2} J_{n+m}(\pm\gamma_n a), \tag{104}$$

$$\left(\rho_\pm^\gamma\right)_{n,m} = i^{m+n+1}\sqrt{\gamma_n} e^{\pm i\gamma_n L/2} J_{n+m}(\pm\gamma_n a), \tag{105}$$

where $\gamma = \{k, q\}$. Just like the coefficient vectors $\boldsymbol{c}$ and $\boldsymbol{d}$, we also write the coefficients α_n and β_n in terms of vectors, i.e., $\boldsymbol{\alpha} = (\dots, \alpha_{-1}, \alpha_0, \alpha_1, \dots)^T$. After rearranging Eqs. (98)-(101) we find the Floquet scattering matrix

$$\begin{pmatrix} \boldsymbol{d_p} \\ \boldsymbol{c_p} \end{pmatrix} = S \begin{pmatrix} \boldsymbol{a_p} \\ \boldsymbol{b_p} \end{pmatrix}, \tag{106}$$

connecting the propagating modes. Note that evanescent modes inside the scattering region, i.e., $\alpha_{n<0}$ and $\beta_{n<0}$, contribute to the Floquet scattering matrix [cf. Eqs. (98)-(101)] since these modes are coupled to flux-carrying propagating modes in the asymptotic regions.

Having now accomplished that, we can identify different FWS operators. We start by examining the FWS operator with respect to V_0, i.e.

$$Q_{V_0} = -iS^\dagger \frac{\mathrm{d}S}{\mathrm{d}V_0}, \tag{107}$$

and derive for its eigenvalues

$$\begin{aligned}\theta_{V_0} &= -\mu\frac{1}{T}\int_0^T \mathrm{d}t\ \langle\Phi_\epsilon|\frac{\mathrm{d}V(x,t)}{\mathrm{d}V_0}|\Phi_\epsilon\rangle \\ &= -\mu\frac{1}{T}\int_0^T \int_{-L/2+x_0}^{L/2+x_0} \mathrm{d}t\,\mathrm{d}x\,|\Phi_\epsilon(x,t)|^2.\end{aligned} \tag{108}$$

We see that the eigenvalues are connected to the temporally averaged probability density inside the barrier. Again transferring this result to the photonic case results in an eigenvalue which is connected to the intensity of the light stored inside the barrier.

The eigenstate corresponding to the most negative eigenvalue thus features the highest probability of being inside the barrier. This can also be seen in Fig. 12 in which the wavefunction exhibits a strong maximum of probability right in the center of the barrier at all times. In contrast to the Dirac delta counterpart (cf. Fig 2), for the rectangular barrier this maximum can be stabilized since inside the scattering region there are also propagating modes present. On the other hand, the state corresponding to the maximal eigenvalue tries to minimize the probability density inside the barrier. As can be seen from Fig. 13, this is achieved by exhibiting local maxima at the borders of the potential such that for a given number of Floquet modes there are as much zeros of the wavefunction as possible inside the barrier.

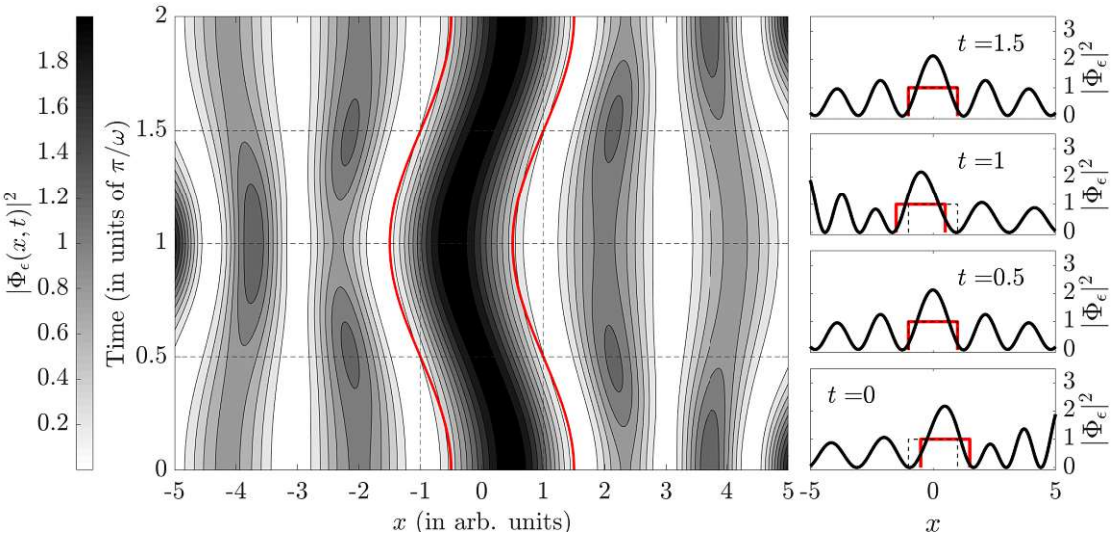

Figure 12: Absolute value of the eigenstate wavefunction $|\Phi_\epsilon(x,t)|^2$ corresponding to the smallest eigenvalue of Q_{V_0}. This state maximizes the probability of finding the electron inside the barrier. The right panels are cuts through the contour plot at the specified times. The red lines indicate the borders of the barrier potential of length $L = 2$. In this plot the parameters take the values $\mu = 1$, $a = 0.5$, $V_0 = 1$, $\epsilon = 0.7$ (arb. units).

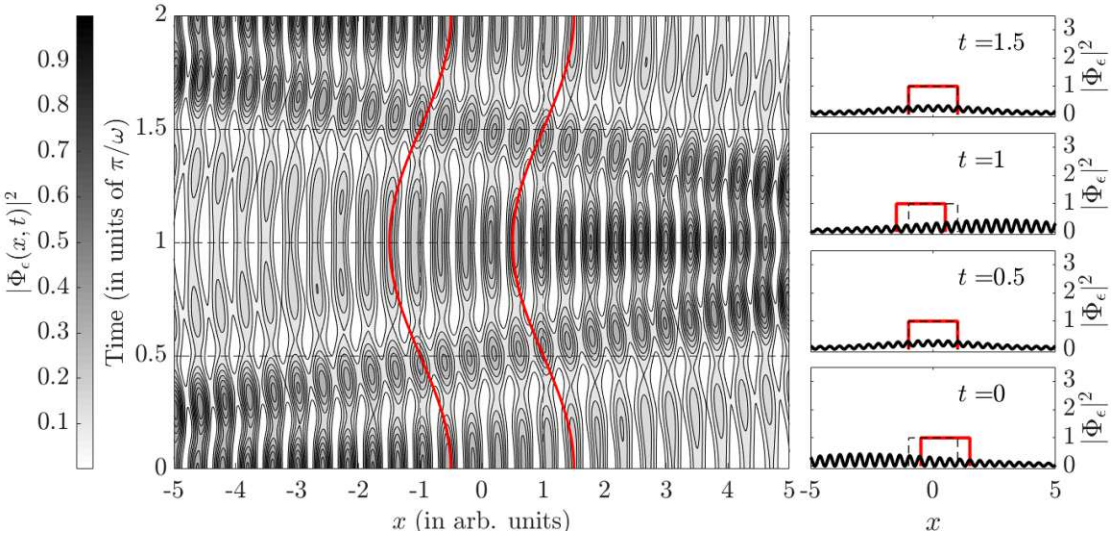

Figure 13: Absolute value of the eigenstate wavefunction $|\Phi_\epsilon(x,t)|^2$ corresponding to the largest eigenvalue of Q_{V_0}. This state minimizes the probability of finding the electron inside the barrier. The right panels are cuts through the contour plot at the specified times. The red lines indicate the borders of the barrier potential of length $L = 2$. In this plot the parameters take the values $\mu = 1$, $a = 0.5$, $V_0 = 1$, $\epsilon = 0.7$ (arb. units).

A further interesting case is the FWS operator with respect to the the amplitude a of the oscillation

$$Q_a = -iS^\dagger \frac{\mathrm{d}S}{\mathrm{d}a}. \tag{109}$$

Similar to the case of the Dirac delta potential oscillating in position in Section 4.1, we expect for the FWS operator Q_a that its eigenvalues correspond to a notion of momentum transfer since a derivative with respect to a spatial coordinate appears in its definition. Applying Eq. (47) for the present case of $\alpha \to a$ leads to

$$\begin{aligned}\theta_a &= -\mu \frac{1}{T}\int_0^T \mathrm{d}t\ \langle\Phi_\epsilon|\frac{\mathrm{d}V(x,t)}{\mathrm{d}a}|\Phi_\epsilon\rangle \\ &= -\mu\frac{V_0}{T}\int_0^T \mathrm{d}t\cos(\omega t)\left[-|\Phi_\epsilon[-L/2 + a\cos(\omega t), t]|^2 + |\Phi_\epsilon[L/2 + a\cos(\omega t), t]|^2\right].\end{aligned} \tag{110}$$

Eq. (110) tells us, that the eigenvalues of the FWS operator correspond to the cosine-weighted, time averaged difference of the absolute value squared of the wavefunction at the borders of the barrier. Figure 14 shows the state corresponding to the smallest eigenvalue. We can clearly see the similarity to the Dirac delta case. Also here for the extended barrier, the eigenstate hits the potential exactly at that moment in time at which the potential is maximally displaced, i.e. at the turning points. This state

therefore is optimal for transferring the maximal amount of momentum to the barrier, where the direction of the momentum transfer again is connected on the cosine weighting factor. Contrary, the state corresponding to the maximal eigenvalue hits the potential also at the turning points just from the other side (not shown). Furthermore, we also want to mention the behaviour of a state corresponding to an eigenvalue close to zero. In that case the absolute value of the wavefunction squared is nearly zero at the borders of the potential at all times and therefore there is nearly no probability of finding the electron there (not shown).

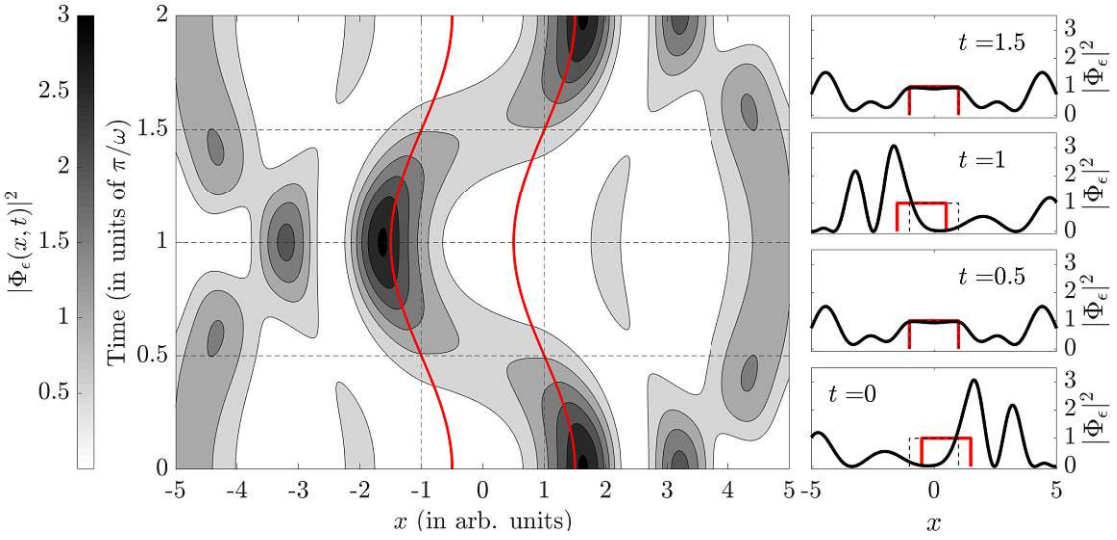

Figure 14: Absolute value of the eigenstate wavefunction $|\Phi_\epsilon(x,t)|^2$ corresponding to the smallest eigenvalue of Q_a. This state hits the potential at the point of maximal displacement, i.e. at the turning points, as it is optimal for decelerating it. The right panels are cuts through the contour plot at the specified times. The red lines indicate the borders of the barrier potential of length $L = 2$. In this plot the parameters take the values $\mu = 1$, $a = 0.5$, $V_0 = 1$, $\epsilon = 0.7$ (arb. units).

Last, we also examine the FWS operator with respect to the length of the barrier, i.e.,

$$Q_L = -iS^\dagger \frac{\mathrm{d}S}{\mathrm{d}L}. \tag{111}$$

We again apply Eq. (47), which results in

$$\begin{aligned}\theta_L &= -\mu \frac{1}{T}\int_0^T \mathrm{d}t\ \langle \Phi_\epsilon | \frac{\mathrm{d}V(x,t)}{\mathrm{d}L} | \Phi_\epsilon \rangle \\ &= -\mu \frac{V_0}{T}\int_0^T \mathrm{d}t\ \frac{1}{2}\Big\{ |\Phi_\epsilon[-L/2 + a\cos(\omega t), t]|^2 + |\Phi_\epsilon[L/2 + a\cos(\omega t), t]|^2 \Big\}.\end{aligned} \tag{112}$$

This means that the eigenvalues correspond to the time averaged sum of the probability density at the borders of the potential. In contrast to the FWS operator Q_{V_0}, the eigenvalues of this operator are connected to the absolute value squared of the wavefunction only at the borders of the potential, resulting in an applied force rather than a maximized probability density (or stored intensity for the photonic case) inside the barrier. The eigenstate corresponding to the smallest eigenvalue is depicted in Fig. 15. This state

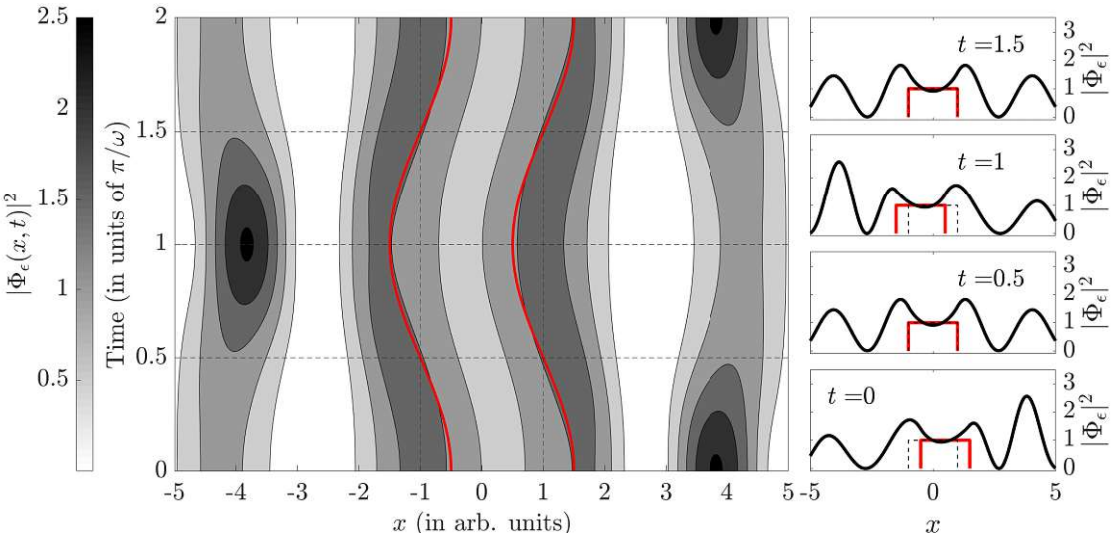

Figure 15: Absolute value of the eigenstate wavefunction $|\Phi_\epsilon(x,t)|^2$ corresponding to the smallest eigenvalue of Q_L. This state maximizes the probability of finding the electron at the borders of the barrier. The right panels are cuts through the contour plot at the specified times. The red lines indicate the borders of the barrier potential of length $L = 2$. In this plot the parameters take the values $\mu = 1$, $a = 0.5$, $V_0 = 1$, $\epsilon = 0.7$ (arb. units).

maximizes the probability for finding the electron right next to the barrier. Transferring this again into a photonic setting means that the light intensity is high at the borders

of the scatterer which in turn increases the reflection probability at the barrier thus applying some pressure from the outside. This effect has been observed in the static, 2D photonic case [6], where the GWS operator with a derivative with respect to the radius of a circular target yields eigenstates which apply a well-defined radial pressure onto the target. On the other hand, a state corresponding to an eigenvalue close to zero, which is in this case also the maximal value of the eigenvalue, minimizes the probability density at the borders of the potential similar to the state corresponding to an eigenvalue close to zero of Q_a.

5.2. Barrier Potential Oscillating in Strength

Analogously to Section 4.2, we want to study the problem of scattering off a potential barrier of height V_0 oscillating around V_0 with an amplitude of V_1. The Floquet scattering matrix has already been derived in [9, 28]. In the following we summarize the main steps. The potential reads

$$\begin{aligned} V(x,t) &= [V_0 + V_1 \cos(\omega t)]\, \Theta(|x| - L/2) \\ &= \begin{cases} V_0 + V_1 \cos(\omega t), & -L/2 < x < L/2, \\ 0, & \text{else}, \end{cases} \end{aligned} \tag{113}$$

where $V_0 + \cos(\omega t) V_1 \in \mathbb{R}$ is the time-dependent strength of the barrier. Again, we make use of the Floquet formalism using the ansatz

$$\Phi_\epsilon(x,t) = \sum_{n=-\infty}^{\infty} \psi_n(x) e^{-i(\epsilon + n\omega)t} \tag{114}$$

for the wavefunction, where

$$\psi_n(x) = \begin{cases} \psi_n^{(I)}(x) & x < -L/2, \\ \sum_{m=-\infty}^{\infty} \psi_m^{(II)}(x) J_{n-m}\left(\frac{V_1}{\omega}\right) & -L/2 < x < L/2, \\ \psi_n^{(III)}(x) & x > L/2, \end{cases} \tag{115}$$

with J_n being the Bessel function of the first kind. Note, that $J_{n-m}(0) = \delta_{m,n}$ causing the recovery of the static uncoupled case for $V_1 \to 0$ since the time-dependence vanishes (to be rigorous, this is also true for $\omega \to \infty$, where the electron cannot resolve the movement anymore). The ansatz for the spatial wavefunction reads

$$\psi_n^{(I)}(x) = \frac{1}{\sqrt{k_n}} \left(a_n e^{ik_n x} + d_n e^{-ik_n x} \right), \tag{116}$$

$$\psi_m^{(II)}(x) = \frac{1}{\sqrt{q_m}} \left(\alpha_m e^{iq_m x} + \beta_m e^{-iq_m x} \right), \tag{117}$$

$$\psi_n^{(III)}(x) = \frac{1}{\sqrt{k_n}} \left(c_n e^{ik_n x} + b_n e^{-ik_n x} \right), \tag{118}$$

where we – in analogy to the previous section – introduced the momentum inside the barrier as

$$q_n = \sqrt{2\mu\,(\epsilon + n\omega - V_0)}. \tag{119}$$

Our goal is now to derive the scattering matrix of this system. For this we demand continuity of the wavefunction and its first derivative at $x = \pm L/2$ leading to

$$M_s^+ (\boldsymbol{\alpha} + \boldsymbol{\beta}) = M_r (\boldsymbol{a} + \boldsymbol{b}), \tag{120}$$

$$M_s^- (\boldsymbol{\alpha} - \boldsymbol{\beta}) = M_r (\boldsymbol{a} - \boldsymbol{b}), \tag{121}$$

$$\boldsymbol{d} = M_c^+ \boldsymbol{\alpha} + M_c^- \boldsymbol{\beta} - M_i \boldsymbol{a}, \tag{122}$$

$$\boldsymbol{c} = M_c^- \boldsymbol{\alpha} + M_c^+ \boldsymbol{\beta} - M_i \boldsymbol{a}. \tag{123}$$

The elements of the matrices appearing in Eqs. (120)-(123) are then given by

$$\left(M_s^{\pm}\right)_{n,m} = \frac{1}{\sqrt{q_m}}\left[(k_n + q_m)\, e^{-iq_m L/2} \pm (k_n \pm q_m)\, e^{iq_m L/2}\right] J_{n-m}\left(\frac{V_1}{\omega}\right), \tag{124}$$

$$\left(M_c^{\pm}\right)_{n,m} = \sqrt{\frac{k_n}{q_m}} e^{-i(k_n \pm q_m)L/2} J_{n-m}\left(\frac{V_1}{\omega}\right), \tag{125}$$

$$\left(M_r\right)_{n,m} = \frac{1}{\sqrt{k_n}} 2k_n e^{-ik_n L/2}\delta_{n,m}, \tag{126}$$

$$\left(M_i\right)_{n,m} = e^{-ik_n L/2}\delta_{n,m}. \tag{127}$$

Rearranging the above equations then again yields the unitary Floquet scattering matrix, which is defined by

$$\begin{pmatrix} \boldsymbol{d_p} \\ \boldsymbol{c_p} \end{pmatrix} = S \begin{pmatrix} \boldsymbol{a_p} \\ \boldsymbol{b_p} \end{pmatrix}. \tag{128}$$

Since the considered potential is defined by three parameters, namely V_0, V_1 and L, in the following we study the FWS operator with a derivative with respect to each of those parameters. We start by investigating the FWS operator with respect to V_0, i.e.

$$Q_{V_0} = -iS^{\dagger}\frac{\mathrm{d}S}{\mathrm{d}V_0}. \tag{129}$$

Its eigenvalues are again connected to the probability density inside the scattering region via

$$\begin{aligned} \theta_{V_0} &= -\mu\frac{1}{T}\int_0^T \mathrm{d}t\ \langle\Phi_\epsilon|\frac{\mathrm{d}V(x,t)}{\mathrm{d}V_0}|\Phi_\epsilon\rangle \\ &= -\mu\frac{1}{T}\int_0^T\int_{-L/2}^{L/2} \mathrm{d}t\,\mathrm{d}x\,|\Phi_\epsilon(x,t)|^2. \end{aligned} \tag{130}$$

Again, transferring this observation to the photonic case, eigenstates of this operator store a well-defined amount of intensity inside the barrier.

In Fig. 16 the eigenstate corresponding to the smallest eigenvalue is depicted. One can clearly see that this maximizes the probability of finding the electron inside the barrier via creating a pronounced peak of the wavefunction right in the center at all times. A state corresponding to the maximal eigenvalue minimizes the probability of finding the electron inside the barrier. As can be seen from Fig. 17 this states exhibits a destructive interference in general and for a given number of Floquet modes as many zeros of the wavefunction as possible inside the barrier, yielding an eigenvalue close to zero.

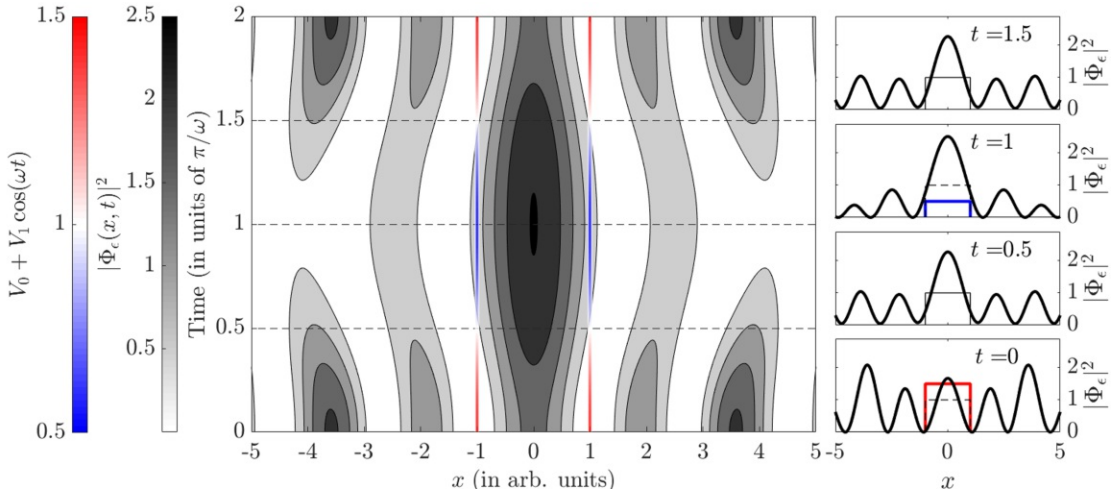

Figure 16: Absolute value of the eigenstate wavefunction $|\Phi_\epsilon(x,t)|^2$ corresponding to the smallest eigenvalue of Q_{V_0} (black to white). This state maximizes the probability of finding the electron inside the barrier potential. The right panels are cuts through the contour plot at the specified times. Red to blue color represents the time-dependent strength of the barrier potential. In this plot the parameters take the values $\mu = 1$, $V_1 = 0.5$, $V_0 = 1$, $L = 2$, $\omega = 1$, $\epsilon = 0.7$ (arb. units).

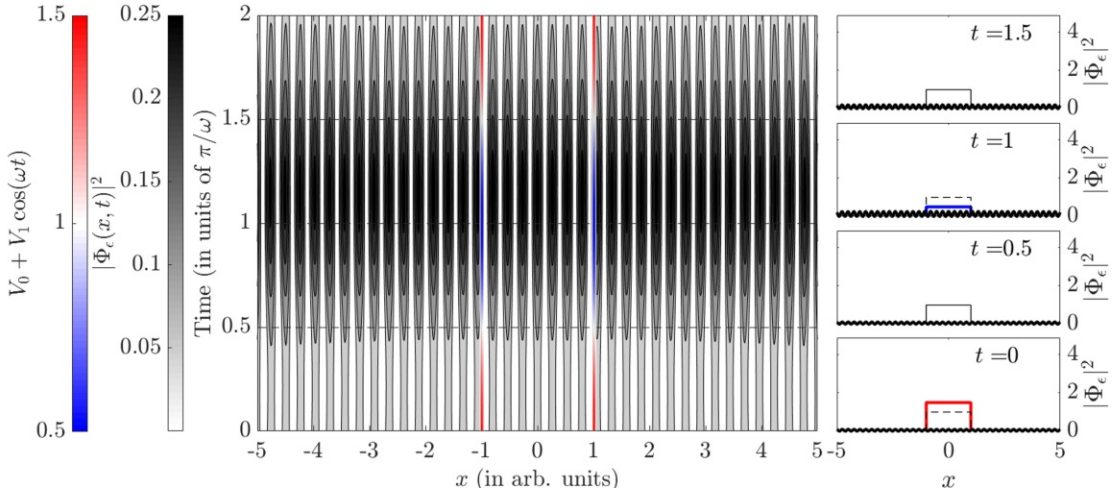

Figure 17: Absolute value of the eigenstate wavefunction $|\Phi_\epsilon(x,t)|^2$ corresponding to the largest eigenvalue of Q_{V_0} (black to white). This state minimizes the probability of finding the electron inside the barrier potential. The right panels are cuts through the contour plot at the specified times. Red to blue color represents the time-dependent strength of the barrier potential. In this plot the parameters take the values $\mu = 1$, $V_1 = 0.5$, $V_0 = 1$, $L = 2$, $\omega = 1$, $\epsilon = 0.7$ (arb. units).

We move on to the FWS operator concerning the height of the oscillation V_1

$$Q_{V_1} = -iS^\dagger \frac{\mathrm{d}S}{\mathrm{d}V_1}. \tag{131}$$

Contrary to the latter case, this operator is connected to the cosine weighted probability density inside the barrier as can be seen by using Eq. (47) with $\alpha \to V_1$ resulting in

$$\begin{aligned} \theta_{V_1} &= -\mu \frac{1}{T} \int_0^T \mathrm{d}t \ \langle\psi| \frac{\mathrm{d}V(x,t)}{\mathrm{d}V_1} |\psi\rangle \\ &= -\mu \frac{1}{T} \int_0^T \int_{-L/2}^{L/2} \mathrm{d}t \, \mathrm{d}x \cos(\omega t) |\psi(x,t)|^2. \end{aligned} \tag{132}$$

Figure 18 shows the state corresponding to the most negative eigenvalue. One can see that this state avoids storing probability of finding the electron inside the barrier at times around $t = j\pi/\omega$, with $j \in \mathbb{N}$, when the cosine term together with the minus sign in front gives an overall large positive contribution. Instead it exhibits a peak around the beginning and end of the period making the integral from Eq. (132) as negative as possible. This means that this state maximizes the probability of finding the electron inside the barrier at times when the strength of the potential is largest. The opposite is the case for the eigenstate corresponding to the most positive eigenvalue, i.e., this state maximizes the electron's probability at times when the strength of the potential is smallest at half of the period. This behaviour is equivalent to what we observed for the respective case for the Dirac delta potential in Section 4.2. It is illustrative to also discuss the state corresponding to an eigenvalue close to zero which is depicted in Fig. 19 (note the different scale in the right panels). It forms peaks of probability density at times, when the cosine term is zero, i.e., $t = j\pi/(2\omega)$, giving no contribution to the time averaging integral in Eq. (132), thus keeping θ_{V_1} as close to zero as possible.

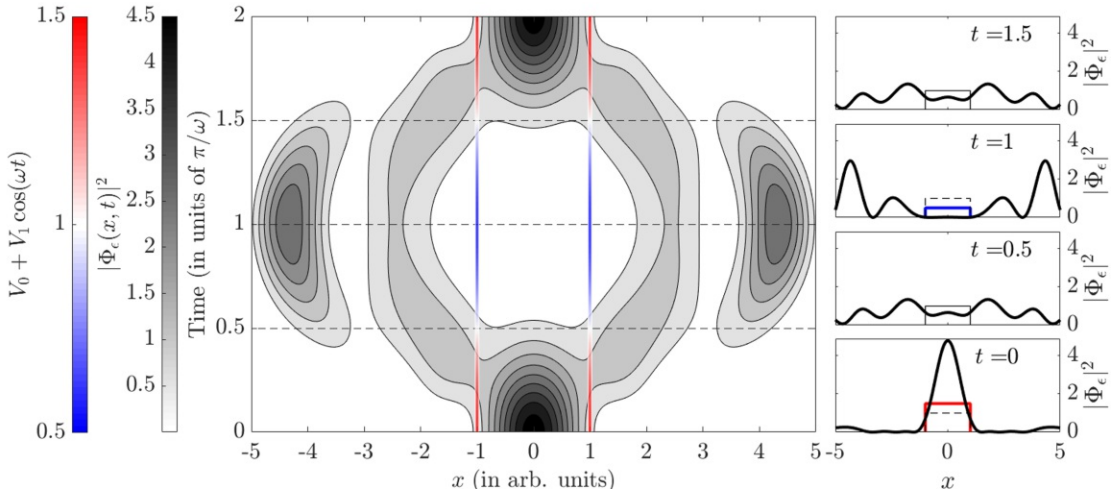

Figure 18: Absolute value of the eigenstate wavefunction $|\Phi_\epsilon(x,t)|^2$ corresponding to the smallest eigenvalue of Q_{V_1} (black to white). This state maximizes the probability of finding the electron inside the barrier at times, when its strength is largest. The right panels are cuts through the contour plot at the specified times. Red to blue color represents the time-dependent strength of the barrier potential. In this plot the parameters take the values $\mu = 1$, $V_1 = 0.5$, $V_0 = 1$, $L = 2$, $\omega = 1$, $\epsilon = 0.7$ (arb. units).

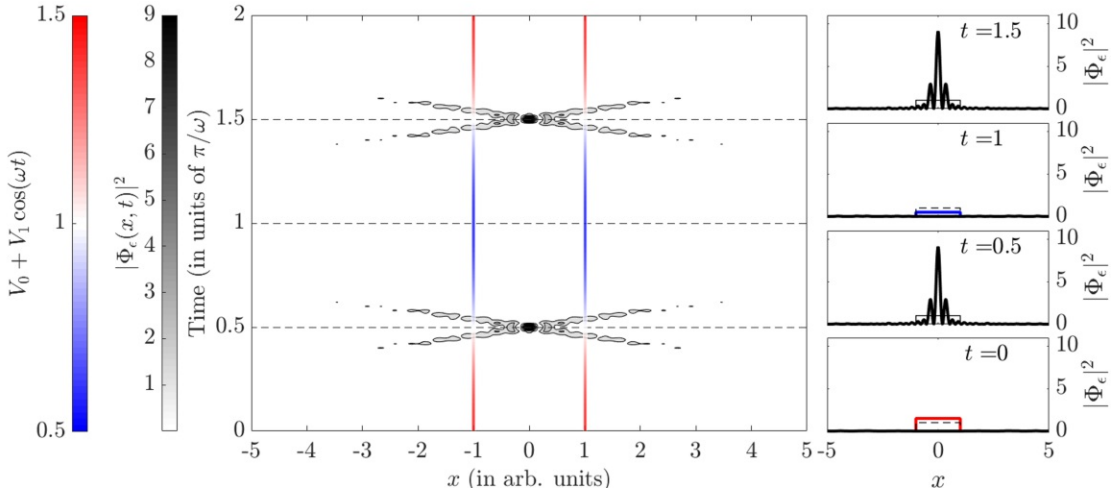

Figure 19: Absolute value of the eigenstate wavefunction $|\Phi_\epsilon(x,t)|^2$ corresponding to an eigenvalue of Q_{V_1} close to zero (black to white). This state maximizes the probability of finding the electron inside the barrier at times, when the weighting factor is zero, i.e., $\cos(\omega t) = 0$. The right panels are cuts through the contour plot at the specified times. Red to blue color represents the time-dependent strength of the barrier potential. In this plot the parameters take the values $\mu = 1$, $V_1 = 0.5$, $V_0 = 1$, $L = 2$, $\omega = 1$, $\epsilon = 0.7$ (arb. units).

Finally, we examine a FWS operator with respect to L, which is given by

$$Q_L = -iS^\dagger \frac{\mathrm{d}S}{\mathrm{d}L}, \tag{133}$$

where the connection between eigenvalues and wavefunction reads

$$\begin{aligned} \theta_L &= -\mu \frac{1}{T} \int_0^T \mathrm{d}t \, \langle \Phi_\epsilon | \frac{\mathrm{d}V(x,t)}{\mathrm{d}L} | \Phi_\epsilon \rangle \\ &= -\mu \frac{1}{T} \int_0^T \mathrm{d}t \, \frac{V_0 + V_1 \cos(\omega t)}{2} \left[|\Phi_\epsilon(-L/2,t)|^2 + |\Phi_\epsilon(L/2,t)|^2 \right]. \end{aligned} \tag{134}$$

Just as in the last subsection [compare Eq. (112)] we observe that a derivative with respect to the length of the barrier is connected to the probability density at the borders of the potential. In this case, however, there is an additional weighting factor present, namely the strength of the potential $V_0 + V_1 \cos(\omega t)$. As can be seen from Fig. 20, this has the effect that the eigenstate corresponding to the smallest eigenvalue always exhibits two peaks at the edges of the potential which are highest at times when the weighting factor is largest. These peaks can again be thought of as applying pressure from the outside onto the barrier.

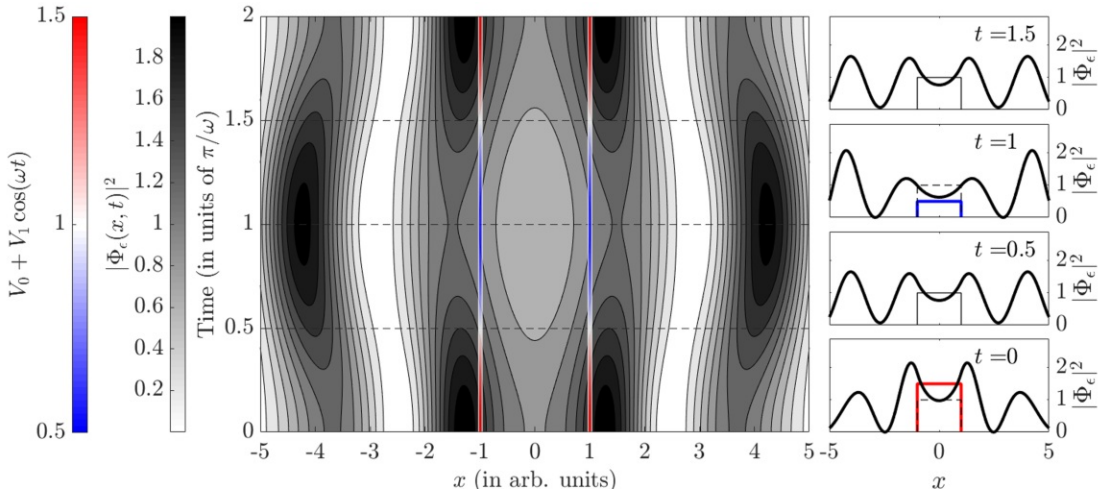

Figure 20: Absolute value of the eigenstate wavefunction $|\Phi_\epsilon(x,t)|^2$ corresponding to the smallest eigenvalue of Q_L (black to white). This state maximizes the probability of finding the electron at the borders of the barrier at times, when its strength is largest. The right panels are cuts through the contour plot at the specified times. Red to blue color represents the time-dependent strength of the barrier potential. In this plot the parameters take the values $\mu = 1$, $V_1 = 0.5$, $V_0 = 1$, $L = 2$, $\omega = 1$, $\epsilon = 0.7$ (arb. units).

If $V_0 < V_1$ there exist also positive eigenvalues θ_L, where the one corresponding to the most positive eigenvalue again forms two peaks, but in this case they are highest at times

when the weighting factor is smallest, i.e., at the beginning an end of the period. It is also interesting to mention the behaviour of an eigenstate which correspond to an eigenvalue close to zero, which exists for all configurations of V_0 and V_1. This state exhibits nearly no probability density in the vicinity of the borders, such that the probability of finding the electron at the borders is nearly zero at all times (cf. Fig. 21).

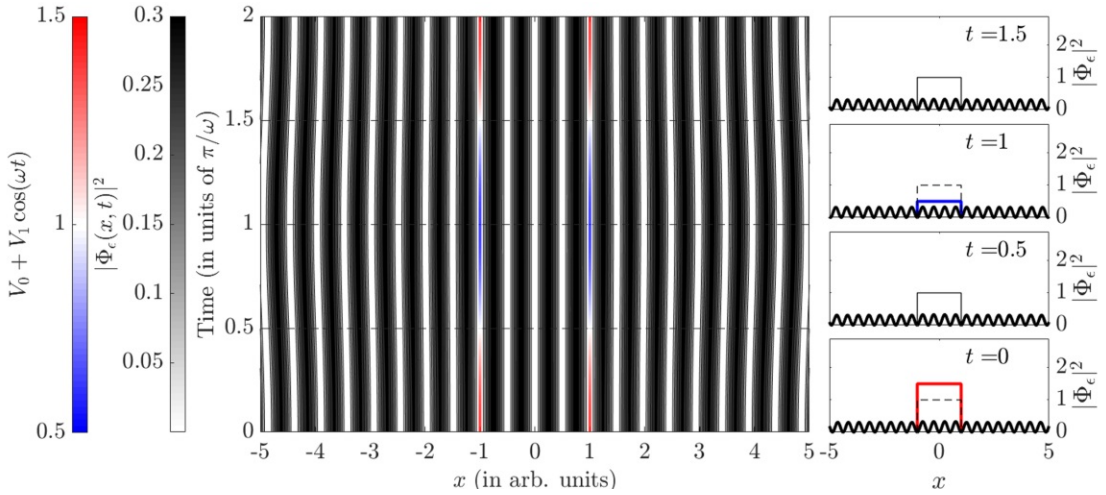

Figure 21: Absolute value of the eigenstate wavefunction $|\Phi_\epsilon(x,t)|^2$ corresponding to the eigenvalue close to zero of Q_L (black to white). This state minimizes the probability of finding the electron at the borders of the barrier at all times. The right panels are cuts through the contour plot at the specified times. Red to blue color represents the time-dependent strength of the barrier potential. In this plot the parameters take the values $\mu = 1$, $V_1 = 0.5$, $V_0 = 1$, $L = 2$, $\omega = 1$, $\epsilon = 0.7$ (arb. units).

6. Conclusion and Outlook

In this work, we extended the concept of the static generalized Wigner-Smith operator to time-periodic 1D systems using Floquet theory. Since for such potentials there exists a time-independent, unitary Floquet scattering matrix, we were able to define a Hermitian Floquet Wigner-Smith (FWS) operator featuring real eigenvalues. We formulated the FWS concept in the field of quantum mechanics since historically the scattering of electrons off time-periodic potentials was studied intensively. We then derived an analytical relation between the eigenvalues of the FWS operator and the probability distribution (or intensity distribution for the photonic case) of the wavefunction inside the potential or at its borders (depending on the considered FWS operator), which enabled us to give the eigenvalues physical meaning and to interpret the temporal behaviour of the corresponding eigenstates. More specifically, we applied the new FWS concept to four different kinds of scattering systems: We investigated a Dirac delta potential oscillating in position or strength and then a potential barrier also oscillating in strength or in position. We were able to show that the eigenstates of the corresponding FWS operator exhibit exiting properties like maximizing the probability density inside the potential or at its borders.

Due to the structural similarity of the Schrödinger and the scalar Helmholtz equation, one can easily transfer the presented results to the photonic case. Considering now the case of classical light fields, the FWS eigenvalues would be a measure for the light intensity stored inside a dielectric particle or the force applied to a certain target. Thus, the FWS concept might be useful for the micromanipulation with classical waves similar to [6], but now in a periodically pulsed manner.

The results found in this thesis indicate that the FWS theory might also be applicable in order to cool particles. We observed that eigenstates of a FWS operator defined with respect to the position of the scatterer are connected to a notion of momentum transfer, which in the end could be used to decelerate or cool particles. Alternatively to using a frozen scattering matrix approach [7], which is only valid in an adiabatic limit, using the FWS concept might open up the possibility to cool particles in more general settings, i.e., without being in a quasi-stationary limit. Similar to cooling, one can of course also think of using the FWS eigenstates corresponding to eigenvalues with the opposite sign in order to accelerate and heat up a collective of particles.

In addition, not only the cooling of an ensemble of classical particles but also controlling and cooling of quantum systems is of great interest, for example, in the field of cavity optomechanics, where the interaction between light and an oscillating cantilever is studied [29]. There, concepts for cooling the mechanical oscillator to its quantum ground state ("ground state cooling") are of great interest [30]. Therefore, transferring the presented results of manipulating oscillating potentials to an optomechanical setting with the aim of controlling a mechanical quantum system might lead to promising ideas.

Moreover, it will also be interesting to study the newly introduced FWS concept in higher dimensions as they give rise to more parameters, thus adding new operator eigenstates to a possible micromanipulation toolbox.

Last, since many real-world settings do not feature any kind of periodicity, which is essential for the Floquet formalism, a future generalization of the GWS and FWS concept to non-periodically time-dependent systems could be very beneficial for applications.

A. Choosing a Proper Cutoff

As mentioned in the main text, for computational reasons one has to truncate to a finite number of Floquet modes. Let us first consider the main dependencies one should be aware of. The cutoff clearly depends critically on the strength of the driving. By increasing the strength of the driving, multiphoton processes get more likely. On the other hand, if we increase the driving frequency (for a fixed strength of the driving), the energy spacing of the Floquet modes increases as well. For multiphoton processes, consequently, more energy is required to occur, making them less likely. These considerations can be summed up into various criteria concerning the cutoff. For example the authors in [10] choose the constrain

$$\left|(S)_{2n_{\mathrm{cut}},n_{\mathrm{cut}}}\right| = |t_{n_{\mathrm{cut}},n_{\mathrm{cut}}}| \approx 1. \tag{135}$$

This means, one should choose that many propagating modes, such that the highest one does not experience any effect from the potential and gets (almost) completely transmitted. In this thesis, we take a different approach.

For a fixed number of outgoing, propagating Floquet modes $n_{\mathrm{cut}}^{\mathrm{out}}$ we choose an appropriate smaller number of incoming, propagating ones $n_{\mathrm{cut}}^{\mathrm{in}} < n_{\mathrm{cut}}^{\mathrm{out}}$. This makes the Floquet scattering matrix a rectangular matrix of dimension $2(n_{\mathrm{cut}}^{\mathrm{out}}+1) \times 2(n_{\mathrm{cut}}^{\mathrm{in}}+1)$. It is important to note that the FWS operator is still a quadratic operator with dimension $2(n_{\mathrm{cut}}^{\mathrm{in}}+1) \times 2(n_{\mathrm{cut}}^{\mathrm{in}}+1)$. This construction allows Floquet modes with a high energy/frequency close to the cutoff $n_{\mathrm{cut}}^{\mathrm{in}}$ to scatter into higher outgoing ones with $n < n_{\mathrm{cut}}^{\mathrm{out}}$. This reduces the amount of incoming flux being lost and therefore keeping the scattering matrix flux-conserving. We now choose $n_{\mathrm{cut}}^{\mathrm{in}}$ such that the FWS operator is approximately Hermitian. Since a Hermitian operator possesses real eigenvalues, we can formulate our cutoff as follows: We decrease the number of incoming modes up to the point where the imaginary part of every eigenvalue of the FWS operator is smaller than a certain cut-off value c_{cut}. For the plots of the wavefunctions presented in this thesis we choose $c_{\mathrm{cut}} = 10^{-5}$.

To illustrate the advantage of this approach, in Fig. 22 we show the deviation of $S^\dagger S$ from the identity matrix as a measure for the unitarity of the Floquet scattering matrix S. In this plot S is based on the barrier potential oscillating in position (cf. Section 5.1). As one can see, for a symmetric cutoff, i.e., $n_{\text{in}} = n_{\text{out}}$, the scattering of modes corresponding to high energies induce a large deviation from the unit matrix. This can be understood as the scattering of these modes into higher ones with $n > n_{\text{out}}$ cannot be described by the quadratic scattering matrix and therefore probability flux is lost which induces a non-unitary scattering matrix. On the contrary, if one chooses an asymmetric cutoff, i.e., $n_{\text{out}} > n_{\text{in}}$, the scattering matrix also keeps track of the scattering behaviour of high incoming modes and thus a unitary Floquet scattering matrix can be achieved.

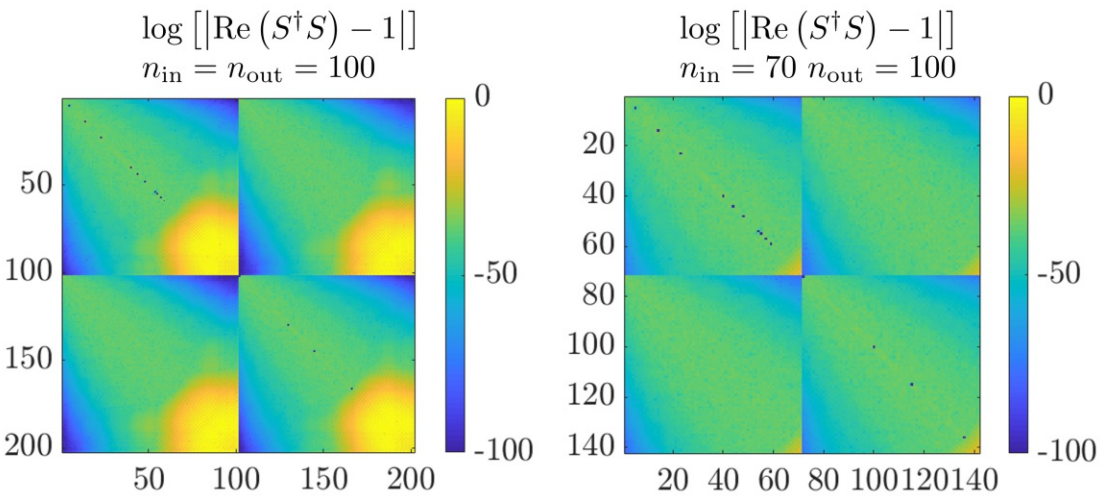

Figure 22: Deviation of the absolute vale of the real part of $S^\dagger S$ from the unit matrix in a logarithmic scale. The Floquet scattering matrix is based on the barrier potential oscillating in position (cf. Section 5.1). For the left plot there are as many input modes as output modes (symmetric cutoff), whereas, for the right plot an asymmetric number of modes is chosen. In both plots the parameters take the values $L = 2$, $\mu = 1$, $a = 0.8$, $V_0 = 1$, $\epsilon = 0.7$ (arb. units).

B. Derivation of Eq. (42)

We want to investigate the connection between the eigenvalues of the static GWS operator and local properties of the wavefunction. Most of the following results have already been derived for the photonic case, for example in [6, 22]. Here we want to transfer those into an electronic system described by a Schrödinger equation. For this, we use the conventions from [23] and follow the discussion in [31].

It is well known that the scattering matrix can be written as

$$\begin{aligned} S &= U^\dagger \left(-1 + 2iw^\dagger \frac{1}{E - H_{\text{in}} + iww^T} w \right) U^\dagger \\ &= U^\dagger \left(-1 + 2iw^T G w \right) U^\dagger. \end{aligned} \tag{136}$$

The unitary diagonal matrix U accounts for the position of the scattering region. Here, E is the energy and μ the mass of the incoming particle and

$$H_{\text{in}} = \frac{p^2}{2\mu} + V \tag{137}$$

is the interaction part of the Hamiltonian of the closed system with the potential $V = V(x, \alpha)$. G is the Green's function and the coupling matrix w accounts for the connection of the scattering region with the asymptotic regions. One should note that w depends on various system parameters, most notably the energy, but one often can neglect these dependencies which we will do in the following. From the unitarity of the scattering matrix it follows that the Green's function obeys the following relation

$$G^\dagger - G = 2iG^\dagger ww^\dagger G. \tag{138}$$

To calculate the derivative of the scattering matrix with respect to a parameter α which appears in the GWS operator, we use the chain rule for matrices [32] and get

$$\frac{\mathrm{d}S}{\mathrm{d}\alpha} = iU^\dagger w^T \frac{\mathrm{d}G}{\mathrm{d}\alpha} w U^\dagger = iU^\dagger w^T G \frac{\mathrm{d}V}{\mathrm{d}\alpha} G w U^\dagger. \tag{139}$$

Putting the above results together, the GWS operator with respect to α becomes

$$\begin{aligned} Q_\alpha &= -iS^\dagger \frac{\mathrm{d}S}{\mathrm{d}\alpha} \\ &= -2Uw^\dagger G^\dagger \frac{\mathrm{d}V}{\mathrm{d}\alpha} G w U^\dagger. \end{aligned} \tag{140}$$

The relation between an ansymptotic state $|\zeta\rangle$ and the wavefunction inside the scattering region $|\chi_\zeta\rangle$ reads

$$|\chi_\zeta\rangle = \sqrt{\frac{2}{\mu}} G w U^\dagger |\zeta\rangle , \tag{141}$$

which finally leads to Eq. (42)

$$\langle\zeta|Q_\alpha|\zeta\rangle = -\mu \langle\chi_\zeta| \frac{\mathrm{d}V}{\mathrm{d}\alpha} |\chi_\zeta\rangle . \tag{142}$$

C. Numerics concerning Eq. (47)

In this Appendix, we provide numerical data to emphasize the excellent agreement between the eigenvalues of the FWS operator and the probability density as stated by Eq. (47). Figure 23 (a) and (b) depict the linear relation between the eigenvalues of the FWS operators discussed for the spatially oscillating Delta potential in Section 4.1 and its respective Floquet expectation value of the derivative of the potential [cf. Eqs. (65) and (69)]. Figure 23 (c) shows this connection for the FWS operator for the Dirac delta potential oscillating in height discussed in Section 4.2 [cf. Eq. (88)].

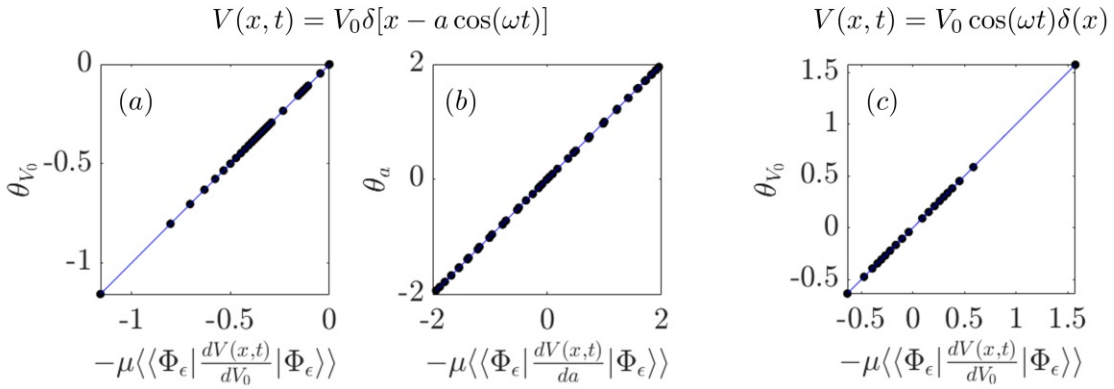

Figure 23: Linear relations between the numerically calculated eigenvalues of different FWS operators and their analytical expressions given by Eq. (47) with the corresponding potential (see $V(x,t)$ in the plot titles). In (a) and (b), the eigenvalues θ_{V_0} and θ_a for a spatially oscillating barrier are shown, respectively. (c) also shows the eigenvalue θ_{V_0}, but for a delta barrier oscillating in strength.
Black dots are the numerical data points and the blue line is the expected relation according to Eq. (47). In all of these plots the parameters (in arb. units) take the values $\mu = 1$, $V_0 = 1$, $\omega = 1$, $\epsilon = 0.7$, and $a = 1$ for the plots (a) and (b).

We present the validity of Eq. (47) for the potential barrier oscillating in position [see for Section 5.1, Eqs. (108), (110), and (112)] in Fig. 24 and for the barrier potential oscillating in strength [see for Section 5.2, Eqs. (130), (132), and (134)] in Fig. 25.

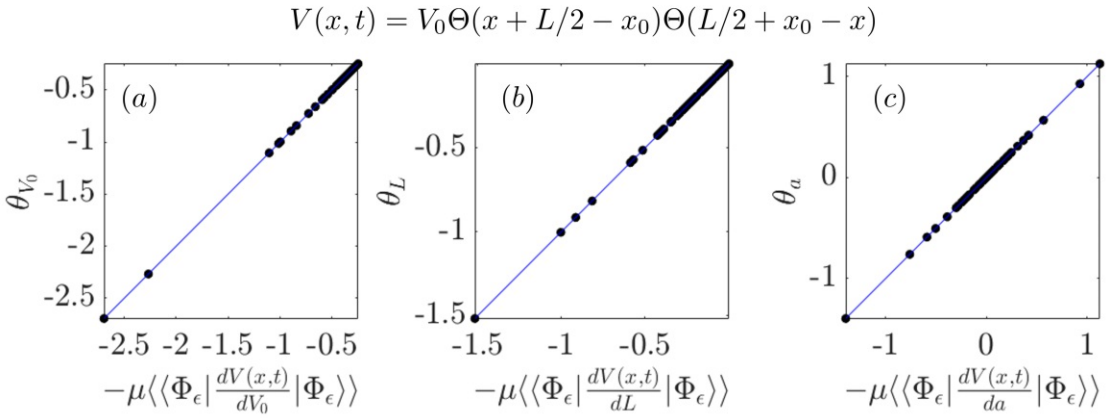

Figure 24: Linear relations between the numerically calculated eigenvalues of different FWS operators and their analytical expressions given by Eq. (47) with $V(x,t)$ specified in the plot title. In (a) eigenvalues θ_{V_0}, in (b) the eigenvalues θ_L, and in (c) the eigenvalues θ_a are shown. Black dots are the numerical data points and the blue line is the expected relation according to Eq. (47). In these plots the parameters take the values $\mu = 1$, $V_0 = 1$, $a = 0.5$, $L = 2$, $\omega = 1$, $\epsilon = 0.7$ (arb. units).

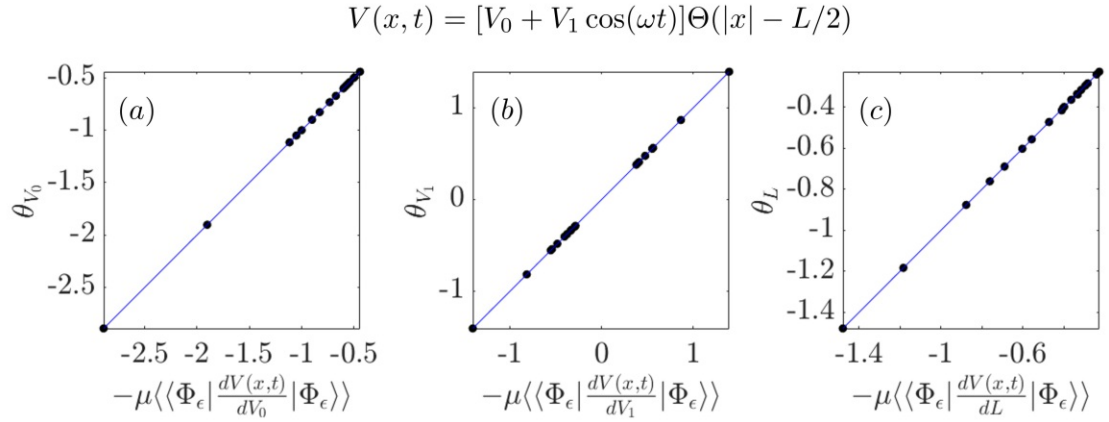

Figure 25: Linear relations between the numerically calculated eigenvalues of different FWS operators and their analytical expressions given by Eq. (47) with $V(x,t)$ specified in the plot title. In (a) the eigenvalue θ_{V_0}, in (b) the eigenvalue θ_{V_1}, and in (c) the eigenvalue θ_L is shown. Black dots are the numerical data points and the blue line is the expected relation according to Eq. (47). In this plots the parameters take the values $\mu = 1$, $V_0 = 1$, $V_1 = 0.5$, $L = 2$, $\omega = 1$, $\epsilon = 0.7$ (arb. units).

D. Derivation of Eq. (68)

We start by considering the well-defined Eq. (110), which connects the eigenvalues θ_a of the spatially oscillating potential barrier to the wavefunction inside the barrier

$$\begin{aligned}\theta_a &= -\mu\frac{1}{T}\int_0^T \mathrm{d}t\ \langle\Phi_\epsilon|\frac{\mathrm{d}V(x,t)}{\mathrm{d}a}|\Phi_\epsilon\rangle \\ &= -\mu\frac{V_0}{T}\int_0^T \mathrm{d}t\cos(\omega t)\left[-|\Phi_\epsilon(-L/2+a\cos(\omega t),t)|^2+|\Phi_\epsilon(L/2+a\cos(\omega t),t)|^2\right].\end{aligned} \tag{143}$$

We want to investigate the Dirac delta limit, which means we substitute

$$V_0 \to \frac{\tilde{V}_0}{\Delta}, \tag{144}$$

$$L \to \Delta, \tag{145}$$

where $\Delta \ll 1$ thus yielding a very short but very high potential. Taking the limit $\Delta \to 0$ then causes the potential barrier to transition into a Dirac delta potential. With this replacement we get

$$\theta_a = -\mu\frac{\tilde{V}_0}{T}\int_0^T \mathrm{d}t\cos(\omega t)\frac{1}{\Delta}\left[-|\psi(x_0-\Delta/2,t)|^2+|\psi(x_0+\Delta/2,t)|^2\right], \tag{146}$$

where $x_0 = a\cos(\omega t)$ as usual. We now expand the probability density around x_0, which leads to

$$\begin{aligned}\theta_a = -\mu\frac{\tilde{V}_0}{T}\int_0^T \mathrm{d}t\cos(\omega t)\frac{1}{\Delta}\Bigg\{ &-\left[|\psi(x_0^-,t)|^2-\frac{\Delta}{2}\frac{\mathrm{d}}{\mathrm{d}x_0}|\psi(x_0^-,t)|^2+\mathcal{O}(\Delta^2)\right] \\ &+\left[|\psi(x_0^+,t)|^2+\frac{\Delta}{2}\frac{\mathrm{d}}{\mathrm{d}x_0}|\psi(x_0^+,t)|^2+\mathcal{O}(\Delta^2)\right]\Bigg\}.\end{aligned} \tag{147}$$

Since the wavefunction is continuous everywhere it holds that $|\psi(x_0^+,t)|^2 = |\psi(x_0^-,t)|^2$ and therefore the zero-order terms cancel out yielding

$$\theta_a = -\mu\frac{\tilde{V}_0}{T}\int_0^T \mathrm{d}t\cos(\omega t)\frac{1}{2}\left[\frac{\mathrm{d}}{\mathrm{d}x_0}|\psi(x_0^-,t)|^2+\frac{\mathrm{d}}{\mathrm{d}x_0}|\psi(x_0^+,t)|^2+\mathcal{O}(\Delta)\right]. \tag{148}$$

Finally, we notice that

$$\frac{\mathrm{d}}{\mathrm{d}a} = \frac{\mathrm{d}x_0}{\mathrm{d}a}\frac{\mathrm{d}}{\mathrm{d}x_0} = \cos(\omega t)\frac{\mathrm{d}}{\mathrm{d}x_0} \tag{149}$$

and by applying the Dirac delta limit $\Delta \to 0$ we arrive at

$$\theta_a = -\mu\frac{\tilde{V}_0}{T}\int_0^T \mathrm{d}t\,\frac{1}{2}\left[\frac{\mathrm{d}}{\mathrm{d}a}|\psi(x_0^-,t)|^2+\frac{\mathrm{d}}{\mathrm{d}a}|\psi(x_0^+,t)|^2\right]. \tag{150}$$

With the re-substitution $\tilde{V}_0 \to V_0$, this coincides exactly with Eq. (69).

Acknowledgements

First and foremost I would like to thank my supervising professor Stefan Rotter for giving me the chance of doing research in his excellent group and providing me guidance throughout this thesis. I want to offer my special gratitude to my co-supervisors Matthias Kühmayer and Matthias Zens, who always offered an open ear and provided constructive remarks in our discussions. I really enjoyed our regular meetings – online and offline – and I deeply appreciate the extraordinary support from all of you. Furthermore, I want to thank Felix Schneider for introducing me to the topic of Floquet scattering and fruitful discussions at an early stage of the thesis.

I also want to thank my colleges of my study group, who became much more than that over to past years, and my friends and family. Finally but most importantly I want to thank my parents and Michaela for supporting me in every possible way.

References

[1] G. Thalhammer et al. "Optical macro-tweezers: trapping of highly motile micro-organisms". In: *Journal of Optics* 13.4 (2011), p. 044024. DOI: 10.1088/2040-8978/13/4/044024.

[2] A. Ashkin et al. "Observation of a single-beam gradient force optical trap for dielectric particles". In: *Opt. Lett.* 11.5 (1986), pp. 288–290. DOI: 10.1364/OL.11.000288.

[3] P. Ambichl et al. "Focusing inside Disordered Media with the Generalized Wigner-Smith Operator". In: *Phys. Rev. Lett.* 119.3 (2017), p. 033903. DOI: 10.1103/PhysRevLett.119.033903.

[4] E. P. Wigner. "Lower Limit for the Energy Derivative of the Scattering Phase Shift". In: *Phys. Rev.* 98.1 (1955), pp. 145–147. DOI: 10.1103/PhysRev.98.145.

[5] F. T. Smith. "Lifetime Matrix in Collision Theory". In: *Phys. Rev.* 118.1 (1960), pp. 349–356. DOI: 10.1103/PhysRev.118.349.

[6] M. Horodynski et al. "Optimal wave fields for micromanipulation in complex scattering environments". In: *Nature Photonics* 14.3 (2020). DOI: 10.1038/s41566-019-0550-z.

[7] M. Kaczvinszki et al. *Optimal Cooling of Multiple Levitated Particles through Far-Field Wavefront-Shaping*. 2021. arXiv: 2103.12592 [physics.optics].

[8] D. F. Martinez and L. E. Reichl. "Transmission properties of the oscillating δ-function potential". In: *Phys. Rev. B* 64.24 (2001), p. 245315. DOI: 10.1103/PhysRevB.64.245315.

[9] W. Li and L. E. Reichl. "Floquet scattering through a time-periodic potential". In: *Phys. Rev. B* 60.23 (1999), pp. 15732–15741. DOI: 10.1103/PhysRevB.60.15732.

[10] A. Emmanouilidou and L. E. Reichl. "Floquet scattering and classical-quantum correspondence in strong time-periodic fields". In: *Phys. Rev. A* 65.3 (2002), p. 033405. DOI: 10.1103/PhysRevA.65.033405.

[11] C. J. Joachain, N. J. Kylstra, and R. M. Potvliege. *Atoms in intense laser fields*. Cambridge: Cambridge University Press, 2011. ISBN: 0511993455.

[12] M. Holthaus. "Floquet engineering with quasienergy bands of periodically driven optical lattices". In: *Journal of Physics B: Atomic, Molecular and Optical Physics* 49.1 (2015), p. 013001. DOI: 10.1088/0953-4075/49/1/013001.

[13] P. Hänggi. "Driven quantum systems". In: *Quantum transport and dissipation*. Ed. by T. Dittrich et al. 1998. ISBN: 3-527-29261-6.

[14] M. Bartelmann et al. *Theoretische Physik 3 / Quantenmechanik*. Berlin, Heidelberg: Springer Berlin Heidelberg Imprint: Springer Spektrum, 2018. ISBN: 3662560720.

[15] W. R. Salzman. "Quantum mechanics of systems periodic in time". In: *Phys. Rev. A* 10.2 (1974), pp. 461–465. DOI: 10.1103/PhysRevA.10.461.

[16] G. Casati and L. Molinari. ""Quantum Chaos" with Time-Periodic Hamiltonians". In: *Progress of Theoretical Physics Supplement* 98 (1989), pp. 287–322. ISSN: 0375-9687. DOI: 10.1143/PTPS.98.287.

[17] G. E. Santoro. *Introduction to Floquet*. URL: https://www.ggi.infn.it/sft/SFT_2019/LectureNotes/Santoro.pdf (visited on 03/02/2021).

[18] T. Bilitewski and N. R. Cooper. "Scattering theory for Floquet-Bloch states". In: *Phys. Rev. A* 91.3 (2015), p. 033601. DOI: 10.1103/PhysRevA.91.033601.

[19] H. Sambe. "Steady States and Quasienergies of a Quantum-Mechanical System in an Oscillating Field". In: *Phys. Rev. A* 7.6 (1973), pp. 2203–2213. DOI: 10.1103/PhysRevA.7.2203.

[20] M. Henseler, T. Dittrich, and K. Richter. "Classical and quantum periodically driven scattering in one dimension". In: *Phys. Rev. E* 64.4 (2001), p. 046218. DOI: 10.1103/PhysRevE.64.046218.

[21] S. Rotter and S. Gigan. "Light fields in complex media: Mesoscopic scattering meets wave control". In: *Rev. Mod. Phys.* 89.1 (2017), p. 015005. DOI: 10.1103/RevModPhys.89.015005.

[22] P. Ambichl. *Coherent wave transport: time-delay and beyond*. PhD thesis. TU Wien, 2016.

[23] L. E. Reichl. *The transition to chaos : in conservative classical systems: quantum manifestations*. Institute for Nonlinear Science. New York, NY [u.a.]: Springer, 1992. ISBN: 0387977538.

[24] G. Zangwill and E. Granot. "Spatial vibrations suppressing resonant tunneling". In: *Phys. Rev. A* 101.1 (2020), p. 012109. DOI: 10.1103/PhysRevA.101.012109.

[25] M. Razavy. *Quantum Theory of Tunneling*. WORLD SCIENTIFIC, 2003. DOI: 10.1142/4984.

[26] S. W. Kim. "Floquet scattering in parametric electron pumps". In: *Phys. Rev. B* 66.23 (2002), p. 235304. DOI: 10.1103/PhysRevB.66.235304.

[27] D. A. Atkinson and H. W. Crater. "An exact treatment of the Dirac delta function potential in the Schrödinger equation". In: *American Journal of Physics* 43.4 (1975), pp. 301–304. DOI: 10.1119/1.9857.

[28] F. Schneider. "Generalized Wigner Smith Operators with Floquet Scattering Matrices". Project Thesis, unpublished.

[29] M. Aspelmeyer, T. J. Kippenberg, and F. Marquardt. "Cavity optomechanics". In: *Rev. Mod. Phys.* 86.4 (2014), pp. 1391–1452. DOI: 10.1103/RevModPhys.86.1391.

[30] J. Millen et al. "Optomechanics with levitated particles". In: *Reports on Progress in Physics* 83.2 (2020), p. 026401. DOI: 10.1088/1361-6633/ab6100.

[31] P. Ambichl. *Delay times and beam-like scattering states in coherent wave transmission through resonators*. Master thesis. TU Wien, 2012.

[32] R. Mathias. "A Chain Rule for Matrix Functions and Applications". In: *SIAM Journal on Matrix Analysis and Applications* 17.3 (1996), pp. 610–620. DOI: 10.1137/S0895479895283409.